Experimental Study on the Slit Glazed Solar Air Heater

Seyed Mahdi Taheri Mousavi

Submitted to the
Institute of Graduate Studies and Research
in partial fulfillment of the requirements for the degree of

Doctor of Philosophy
in
Mechanical Engineering

Eastern Mediterranean University
December 2017
Gazimağusa, North Cyprus

Approval of the Institute of Graduate Studies and Research

Assoc. Prof. Dr. Ali Hakan Ulusoy
Acting Director

I certify that this thesis satisfies the requirements as a thesis for the degree of Doctor of Philosophy in Mechanical Engineering.

Assoc. Prof. Dr. Hasan Hacişevki
Chair, Department of Mechanical Engineering

I certify that I have read this thesis and that in our opinion it is fully adequate in scope and quality as a thesis for the degree of Doctor of Philosophy in Mechanical Engineering.

Prof. Dr. Fuat Egelioğlu
Supervisor

Examining Committee

1. Prof. Dr. Kahraman Albayrak
2. Prof. Dr. Senol Baskaya
3. Prof. Dr. Fuat Egelioğlu
4. Prof. Dr. Mustafa Ilkan
5. Assoc. Prof. Dr. Hasan Hacişevki

ABSTRACT

The energy demand all over the world has been continuously increased. The ever increasing cost, limited resources and possible environmental risks of using conventional energy resources have increased the renewable energy utilization. Solar energy is considered the most promising, inexhaustible and plentiful renewable source of energy. Solar collectors are employed in converting solar energy into thermal energy. The energy consumption of space heating in residential and industrial sector is considerable. In solar energy utilization direct use for space heating could be achieved by employing solar air heaters (SAHs). Technical feasibility has been achieved for SAHs. One of the main concerns is providing economic feasibility.

The present study consists of three series of experiments. First, three SGSAHs with different bed heights (7 cm, 5 cm, and 3 cm) were fabricated with multiple glass panes used for glazing. The length, width, and thickness of each pane were 131 cm, 6 cm and 0.4 cm respectively. The mass flow rate was varied between (0.014 and 0.057) kg/s. The second series of experiments had been conducted to investigate the effect of the width of glass panes, the distance between the slits and mass flow rates on the efficiencies of the three SGSAHs. A glass pane with the length of 131 cm and thickness 0.4 cm was studied for three different glass pane widths: 6 cm, 5 cm, and 4 cm. In addition, the bed height of duct in the second series of experiments was fixed at 7 cm. The ambient air was continuously withdrawn through the gaps between the glass panes by fans. In the first and second series, the experiments were conducted for four different gap distances between the glass panes (i.e., 0.5 mm, 1 mm, 2 mm

and 3 mm). Finally, the third series of experiments had been carried out on a SGSAH and a UTC to compare their efficiencies. The mass flow rates in the second and third series of experiments were varied between (0.014 and 0.029) kg/s.

In the first series of experiments the highest efficiency obtained was 82% where the bed height was 7 cm, glass pane gap distance was 0.5 mm, and the mass flow rate was 0.057 kg/s. The air temperature difference between the inlet and outlet (ΔT) was maximum (27˚C) at the lowest mass flow rate (i.e., 0.014 kg/s) for the same SGSAH. The results demonstrated that for mass flow rates lower than 0.036 kg/s and gap distances greater than 2 mm, the performance of the SGSAH with 3 cm bed height was better compared to the SGSAHs having 5 cm and 7 cm bed heights. However, for flow rates equal or higher than 0.036 kg/s, the SGSAH with 7 cm bed height performed better for all different gap distances compared to the other two SGSAHs. The experimental results of the second series indicated that the maximum thermal efficiency of 75% was obtained when the gap distance was 0.5 mm, slit width was 4 cm and the mass flow rate was 0.029 kg/s. The maximum rise in air temperature was noted as 28℃ at the lowest mass flow rate where the gap distance and slit widths were 0.5 mm and 4 cm respectively. The experimental results obtained from the last series indicated that the thermal efficiency of the SGSAH was 16% higher than the UTC's efficiency.

Keywords: Slit glazed solar air heater, thermal efficiency, unglazed transpired collector, bed height.

ÖZ

Dünyada enerjiye olan talep sürekli artmaktadır. Sürekli artan maliyetler, sınırlı kaynaklar ve geleneksel enerji kaynaklarının kullanılmasıyla ilgili olası çevresel riskler, yenilenebilir enerji kullanımını arttırmıştır. Güneş enerjisi, en umut verici, tükenmez ve bol miktarda yenilenebilir enerji kaynağı olarak kabul edilmektedir. Güneş kollektörleri, ışın enerjisini termal enerjiye dönüştürmekte kullanılırlar. Konut ve sanayi sektöründe, alan ısıtmadaki enerji tüketimi kaydadeğerdir. Güneş enerjisi kullanımında, güneş hava ısıtıcıları kullanılarak doğrudan mekan ısıtması sağlanabilir. Güneş hava ısıtıcıları için teknik fizibilite sağlanmıştır. Ekonomik fizibilite sağlanması ana kaygılardan biridir.

Bu çalışmada, aralıklı cam levhalarla örtülü yeni bir güneşli hava ısıtıcısı tasarımı olan, ve siyah renkli delikli yutuculu geçirgen örtüsüz güneş hava ısıtıcısının performansları deneysel olarak araştırılmıştır. Bu çalışma üç seri deneyden oluşmaktadır. İlk olarak, farklı yatak yükseklikleri (7 cm, 5 cm ve 3 cm) olan üç adet, geçirgen örtüleri aralıklı çoklu cam levhadan oluşan güneş hava ısıtıcısı imal edilmiştir. Her cam levhanın uzunluğu, genişliği ve kalınlığı sırasıyla 131 cm, 6 cm ve 0.4 cm idi. Kütle akışı hızı 0.014 ve 0.057 kg/s arasında değiştirildi. Deneylerin ikinci serisi, cam levhaların genişliği, levhalar arasındaki dar aralık mesafelerinin ve kütle akış hızlarının, aralıklı geçirgen örtülü güneş hava ısıtıcılarının verimliliği üzerindeki etkilerini araştırmak için gerçekleştirildi. Uzunluğu 131 cm, kalınlığı 0.4 cm olan üç farklı cam levha genişliği 6 cm, 5 cm ve 4 cm çalışıldı. Buna ek olarak, ikinci deney dizisindeki kanalın yatak yüksekliği 7 cm'de sabitlenmiştir. Dış ortam havası, cam levhalar arasındaki dar aralıklardan fanlarla sürekli olarak çekildi.

Birinci ve ikinci seride, deneyler cam levhalar arasındaki dört farklı dar aralık mesafesi (0.5 mm, 1 mm, 2 mm ve 3 mm) için gerçekleştirildi. Son olarak, üçüncü deney serisinde, aralıklı geçirgen örtülü güneş hava ısıtıcısı ve ve siyah renkli delikli yutuculu geçirgen örtüsüz güneş hava ısıtıcısının verimlilikleri deneysel olarak karşılaştırıldı. Deneylerin ikinci ve üçüncü serilerinde kütle akış hızı, 0.014 ve 0.029 kg/s arasında değiştirildi.

Birinci deney serisinde, en yüksek verimlilik, yatak yüksekliği 7 cm, cam levha arlarındaki mesafe 0.5 mm ve kütle akış hızı 0.057 kg/s iken, %82 olarak elde edildi. Aynı aralıklı geçirgen örtülü güneş hava ısıtıcısında, giriş ve çıkış arasındaki azami hava sıcaklığı farkı en düşük kütle akış hızında (0.014 kg/s) 27˚C olarak elde edildi. Sonuçlar, kütle akış hızının 0.036 kg/s'den daha az ve cam levha arasındaki mesafelerin 2 mm'den daha fazla oduğu çalışmalarda, yatak yüksekliği 3 cm olan aralıklı geçirgen örtülü güneş hava ısıtıcısı performansının, 5 cm ve 7 cm yatak yüksekliği olan ısıtıcılara kıyasla daha iyi olduğunu göstermiştir. Bununla birlikte, akış hızı 0.036 kg/s'ye eşit veya daha yüksek olduğunda, 7 cm yatak yüksekliğindeki aralıklı geçirgen örtülü güneş hava ısıtıcısı diğer iki ısıtıcıya kıyasla tüm farklı aralık mesafeleri için daha iyi sonuç vermiştir. İkinci serinin deney sonuçları, cam levhalar arasındaki mesafenin 0.5 mm, cam levha genişliğinin 4 cm ve kütle akış hızı 0.029 kg/s olduğu zaman %75'lik azami ısıl verimin elde edildiğini gösterdi. Hava sıcaklığındaki azami artış, cam levhalar arasındaki mesafenin ve levha genişliklerinin sırasıyla 0.5 mm ve 4 cm olduğunda ve en düşük kütle akış hızında 28°C olarak kaydedildi. Son seriden elde edilen deneysel sonuçlar, aralıklı geçirgen örtülü güneş hava ısıtıcısının termal verimliliğinin siyah renkli delikli yutuculu geçirgen örtüsüz güneş hava ısıtıcısının verimliliğinden %16 daha yüksek olduğunu gösterdi.

Anahtar Kelimeler: aralıklı geçirgen örtülü güneş hava ısıtıcısı, termal verimlilik, delikli yutuculu geçirgen örtüsüz güneş hava ısıtıcısı, yatak yüksekliği.

ACKNOWLEDGMENT

I would like to express my sincere gratitude to my supervisor Prof. Dr. Fuat Egelioglu for the continuous support of my PhD study and research. My sincere gratitude also go to the department chair Assoc. Prof. Dr. Hasan Hacişevki for his support, and consideration.

TABLE OF CONTENTS

LIST OF TABLES

LIST OF FIGURES

LIST OF ABBREVIATIONS

Nomenclature

A	Area of the collector (m^2)
C_p	Specific heat capacity(kJ/kgK)
d/w	Relative gap position
G_d/L_v	Relative gap distance
g/e	Relative gap width
g/p	Groove position to pitch ratio
H	Channel height (m)
I	Solar radiation intensity (W/m^2)
P_s	Streamwise pitch spacing of wing/groove (m)
P_t	Transverse pitch spacing of wing (m)
T	Temperature (℃)
t	Time (s)
V	Velocity (m/s)
W/H	Duct aspect ratio
W/w	Relative roughness width
Greek Symbols	Relative roughness width
ΔT	Temperature difference ($T_{out} - T_{in}$)(℃)
ρ	Density of air (kg/m^3)
η	Efficiency of the solar air heater $\eta = \dot{m}C_p\Delta T/IA_c$

μ	Viscosity of air (Ns/m^2)

Subscripts

Air	Film temperature
D_h	Hydraulic diameter
d_p	Plenum height
F	Film
Gd	Gap distance
gp	Glass pane
in	Inlet
out	Outlet
pl	Plenum air
suc	Suction
sp	Side plates of plenum
sw	Slit width
t	Gap distance
W	Absorber width

Abbreviation

GSAH	Glazed solar air heater
GUC	Glazed un-transpired collector
SAH	Solar air heater
SGSAH	Solar glazed solar air heater
UTC	Unglazed transpired collector

Chapter 1

INTRODUCTION

1.1 Background and Problem Description

The main sources of energy in the world are definitely fossil fuels (oil, coal and natural gas), nuclear power and renewables. 80% of the energy consumption is from the fossil fuels. Nuclear power supply a little more than 6% and renewable energy sources has contribution about 14%. It should be considered that the renewables can be categorized by traditional biomass and large hydro which produce 85% and 15% (or slightly more than 2% of the total world consumption energy) by the new renewables (wind and solar energy) (UNDP, 2000).

The energy demand on the world has roughly doubled since 1980. It increases still another 85% until 2050 if the present propensities retain. Investigations show that with these tendencies the energy demands and CO_2 emissions will be doubled. In addition, these conditions will increase the average worldwide temperature a 6°C more until 2050. Energy Technology Perspectives (ETP) 2012 manifests three dramatically various energy futures: the 2°C Scenario, an image of a sustainable energy system; the 4°C Scenario, an evaluation of what introduced policies can offer; and the 6°C Scenario, which is where the world is now proceeding, with potentially destructive results. The principal purpose of global policy is achieving the worldwide target of restricting the long-term raise of the global mean temperature to 2°C. The ETP 2012 2°C Scenario (2DS) considers the technology possibilities required to

realize an ecological future depending on higher energy efficiency and a more balanced energy system, featuring renewable energy sources and lower emissions (International Energy Agency, 2012).

The main greenhouse gas obviously contained in global's atmosphere is water vapour. Subsequent in significance is carbon dioxide (CO_2), followed by methane (CH_4) and nitrous oxide (N_2O). The concentrations of these gases in the atmosphere prior to the start of the industrial revolution kept the mean global surface air temperature about 33 degrees Celsius warmer than it might have been in absence of an atmosphere with such natural amounts of greenhouse gases. Human activity has not significantly effect on the water vapour. In addition, the main anthropogenic greenhouse gas emissions are those of carbon dioxide (CO_2), which occurs mostly from combustion of fossil and biomass fuels and from deforestation.

Hanemann et al. (Hanemann, Labeaga, & López-otero, 2013) indicated that the main part of energy demand in residential buildings is space heating. Energy consumption of building in European Union (EU) increased from 37% to 41% from 1990 to 2010, 14% of which was consumed in non-residential buildings and 27% in residential buildings (Ahern & Norton, 2015). Investigation into the national CO_2 emissions of China indicated that the residential building has 10.3% contribution to 2012 (Fan, Yu, & Wei, 2015). Space heating is 32% and 33% of the total energy use respectively in residential and commercial buildings and also 10% of total direct energy-related CO_2 emissions (Ürge-Vorsatz, Cabeza, Serrano, Barreneche, & Petrichenko, 2015). The energy efficiency for households has increased by 1.8%/year from 2000 and the most improvements have been recorded for space heating as 20% (Bosseboeuf, Gynther, Lapillonne, & Pollier, 2015).

The thermal efficiency of the buildings should be improved and buildings require to incorporate much more energy-efficient building technologies for heating, ventilation and air conditioning (HVAC) technologies; high-efficiency lighting, appliances and tools; and low-carbon or carbon-free technologies, such as heat pumps and solar energy, for space and water heating and cooling (International Energy Agency, 2012). Renewable energy sources (including biomass, solar, wind, geothermal, and hydropower) which use natural resources have the potential to supply energy services with zero or almost zero emissions of both air pollutants and greenhouse gases.

Nowadays, many efforts have been conducted on the sustainable technologies to reduce greenhouse emissions (Sims, 2003). Renewable energy systems are the ones resources which may be employed to supply energy from a natural source that is not depleted when used, e.g. solar energy, wind energy, etc., which can provide energy with zero emissions of both CO_2 and pollutants (UNDP, 2000).

Solar energy is considered the most plentiful one of the renewable energy and available in both direct and indirect types. The Sun's ray emits energy at a rate of 0.8×10^{23} kW, of which, approximately 1.8×10^{14} kW is intercepted by the earth (Thirugnanasambandam, Iniyan, & Goic, 2010). Solar energy could be transforming into thermal energy through the use of solar collector. There are two characteristics which can introduce solar air heaters (SAHs) as an inexpensive and having long life due to their inherent simplicity. SAH is performing as a heat exchanger that converts solar energy into heat. A conventional flat plate SAH is usually made of glazing, solar absorber plate mounted on insulated back surface. One of the primary drawbacks of SAHs is their remarkably low efficiency due to the low density,

volumetric heat capacity and thermal conductivity of air causing to low coefficients of convective heat transfer from solar energy to the air.

The most important applications of SAHs are space heating, seasoning of timber, curing of industrial products, and these can also be effectively utilized for drying of concrete building components. Due to low materials in construction and cost, SAH is introduced as one of the major alternative between the solar air heating systems (Varun, Saini, & Singal, 2007). The applications of solar energy to heat the fluids can include drying vegetables, fruits, meats, eggs incubation, and other industrial purposes (Alkilani, Sopian, Mat, & Alghoul, 2009). Another application of SAHs is integrated with photovoltaic (PV) system to produce energy and electricity, which are called as photovoltaic thermal (PV/T) collectors (Joshi & Tiwari, 2007).

1.2 Aims of Thesis

There are many experimental and numerical investigations to improve the thermal performance of the SAH. To the best of our knowledge, no experiments have been performed with the slit glazed solar air heater (SGSAH). The main aims of this investigation were to determine the effect of different gap distances between the slits glazed, width of slits and bed heights of the collector on the thermal performance by varying the air mass flow rates.

In the SGSAH system, air is pre-heated by passing through slit glazed similar to as in the perforated glazed in the unglazed transpired collector (UTC). With this new design of SAH, advantages of both glazed transpired collector (GUC) and UTC can be combined, i.e., having glass as the glazed cover and slit glazed as semi-transpired, respectively, thereby improving the performance of SAHs.

The main objectives of this experimental research are briefly introduced as follows:

1. To fabricate and test three collectors of mentioned type of SAH.
2. Investigating the effect of bed heights of the collectors on the thermal efficiency and temperature different.
3. Investigating the effect of the width of slits glass panes on the thermal performance of the SGSAH.
4. Accomplishing research for the different gap distances between slits.
5. To construct and test the unglazed transpired collector (UTC).
6. To assess the performance of the collectors by different units and feasibility of the collectors for the North Cyprus environment.

A new design of solar air heating system is proposed in order to minimize the heat losses from glazing. The aim of the study was to design, construct and experimentally investigate SGSAHs with glass panes used as cover plates as they have many advantages over Plexiglas. Glass pane perforation is a costly process and prone to breakage (glass being fragile). To overcome this, air is withdrawn through the gaps between the glass panes rather than circular perforations. In addition, the aim of this study is to construct a cheap and an efficient SAH where the same materials used as in a conventional SAH.

1.3 Thesis Organisation

The main aims and motivations of the present study are introduced in Chapter 1. In Chapter 2, the literature review of previous studies related to SAH is presented. The experiment is defined and experimental apparatuses are described in Chapter 3. The theoretical model of SGSAH is detailed in Chapter 4. The experiments results are

presented in Chapter 4 which includes the effect of bed heights and gap distances, the effect of various slit widths and gap distances on the thermal performance of the collectors and the compression between the experiment results of SGSAH and UTC are shown. In Chapter 5, the general conclusion, discussion and recommendation are demonstrated.

Chapter 2

LITERATURE REVIEW

2.1 Introduction

There is no any specific method of classifying the SAH's type. It can be categorized related to parameters, which have effect on the performance of the collector such as: cover plate, the material of the absorber plate, absorber flow pattern, absorber shapes and flow shapes, or the application of the collector. In this survey, SAHs are classified according the cover plate (glazed solar air heater (GSAH) and unglazed solar air heater (USAH)) and the applications of SAH.

2.1.1 Glazed Solar Air Heater (GSAH)

Many researches were investigated GSAHs aiming to reduce the heat losses from collectors by considering the material of cover plates. In GSAH collectors, sun rays penetrating trough the cover plate and it is absorbed by the absorber plate which placed under cover plate. The amount of heat convection loses from GSAH is lower in compression to unglazed collectors due to its surface temperature is lower than unglazed types. One of the ways to improve thermal performance of solar air heater is to decrease the temperature of absorber plate by increasing the contact area between air and absorber plate.

2.1.1.1 Cover Plate Configuration and Flow Pattern

In a double glazed system, there are two channels where in lower channel air forced between absorbing plate and the first glass while in the upper channel air is in the stagnant and all sides are insulated to prevent heat loss from this channel to

environment. Bhargava et al. (Bhargava, Jha, & Gar, 1990) conducted an analysis by removing insulation from top and bottom sides of a two glazed system and allowed air to flow by natural convection. It was shown that, if no insulation utilized in upper channel, the efficiency of lower channel would not decrease more than 5% compared to case where air is stagnant in upper channel and there is no natural flow.

The results of an experimental study conducted by Wazed et al. (Wazed, Nukman, & Islam, 2010) on the double glazed SAH with forced and natural air flow demonstrated that the maximum room temperature and the temperature difference from ambient were 45.5℃ and 12.25℃ for forced circulation and 41.75℃ and 8.5℃ for natural circulation respectively. Garg et al. (H.P, Garg, V.K, Sharma, R.B, Mahajan, And, Bhargave, 1985) investigated an experiment consists of a flat plate collector in single and double glass types connected with an integrated rock storage and collection system. Results indicated that augmented integrated rock system with double glass is more efficient and storage is effective normally up to 3.30 pm irrespective of mass flow rate. Bhargava et al. (A. K. Bhargava, H. P. Garg, 1985) utilized a computer model to validate the experimental and numerical results.

Plastic cover has relatively light weight, better shatter resistance, and better solar transmission relative to glass. Plastics such as polymethyl methacrylate (known as Plexiglas), polyethylene terephtalate (or Mylar), and polyvinyl fluoride (also called Tedlar) are more suitable than glass for use as the transparent cover in the collector. But, the most disadvantage of Plexiglas compared to glass is the price and deterioration of it by time.

The effect of different glazing material, double glass (DG), single glass (SG), and polymethyl methacrylate (PMMA) on the performance of the collector were investigated experimentally by Das and Chakraverty (Das & Chakraverty, 1991). Results indicated that the temperature raise of DG was 1℃ and 2℃ higher than the collectors with SG and PMMA at the same environmental conditions, respectively. The thermal efficiency of collectors with DG, SG and PMMA covers was achieved 46%, 42%, and 36.5%, respectively. Njomo (Njomo, 1991) used a plastic (Plexiglas) instead of glass cover in the collector and numerical results indicated that the outlet air temperature and the thermal efficiency of the SAH decrease with increasing air channel depth. The low cost, single, and double glazed SAH with and without packed bed consisted of iron chips was investigated experimentally by Gill et al. (Gill, Singh, & Singh, 2012). The thermal efficiencies of packed bed, double glazed, and single glazed were 71.68%, 45.05% and 30.29% respectively at the mass flow rate of 0.02 $m^3/s.m^2$. Esen et al. (Esen, Ozgen, Esen, & Sengur, 2009a) established a modeling study of double pass flow SAH system by using least-squares support vector machine (LS-SVM) method. The experiments carried out at two mass flow rates as 0.03 and 0.05 for three different types of collector with/without ribs on the absorber plate. Comparison between predicted and experimental results indicates that the proposed LS-SVM model can be used for estimating the efficiency of SAHs with appropriate accuracy. Also, the same system was studied numerically with artificial neural network (ANN) and wavelet neural network (WNN) methods. The predicted and experimental results had good agreement (Esen, Ozgen, Esen, & Sengur, 2009b). An experimental study was conducted on a SAH by Al-kayiem and Yassen (Al-kayiem & Yassen, 2015) to evaluate and justify the available correlations was introduced by available correlations. The efficiency of the collector at the tilt angle

of 50° was 2.6% and 3.6% higher than the efficiency of the collector at tilt angles 30° and 70°, respectively. Yeh and Ho (H.-M. Yeh & Ho, 2009) conducted a theoretical study to obtain the effect of recycle on the SAH. It was found that the thermal performance increases with increasing reflux ratio, especially for operating at lower air flow rate with lower inlet air temperature. Also, the highest improvement achieved than 80% at the lowest mass flow rate of 0.01 kg/s. Toğrul and Pehlıvan (Türk Toğrul & Pehlıvan, 2003) investigated experimentally the effect of tilting angle and flow rate on the thermal performance of a SAH having a conical concentrator. The highest thermal efficiency and air outlet temperature are 50% and 82℃ respectively at lowest tilting angle of 28.4° and mass flow rate of 30 kg/hr. In addition, the thermal efficiencies achieved by the conical SAH are close, but the outlet temperatures are approximately twice those reported for conventional flat plate collectors. Later, same authors (Toğrul & Pehlivan, 2005) added a selective absorbing surface and packing in the two-pass airflow passage of the absorbing tube in their novel design. The results indicated that the thermal efficiency of SAH increases by employing selective surface or packing material on the absorber tube compared to SAH without both parameters. It was obtained that the heat transfer coefficient was achieved 240 W/m^2K with cooperating the aluminium wire mesh packing in the absorber tube, while it was 26 W/m^2K at the SAH for empty airflow passage of the absorbing tub. An experimental study carried out by Nemś and Kasperski (Nemś & Kasperski, 2016) on concentrated SAH having internal multiple-fin array. The aim at the study was to verify the previously created mathematical model (Kasperski & Nemś, 2013) of heat transfer processes. The experimental results showed that there is good agreement with the mathematical model. Also, the thermal efficiency varied between 22.7% and 42%. Garg et al. (Garg, Datta, &

Bhargava, 1984) conducted an experimental study of double pass SAH and showed that there is a nonlinear relation between the depth of collector and the thermal efficiency. Also by increasing mass flow rate, the thermal efficiency is increased and outlet temperature decreased. Satcunanathan and Deonarine (Satcunanathan & Deonarine, 1973) showed that the temperature of the glass cover of double pass is decreased 4-10℃ in comparison to the single pass collector. In addition, the thermal performance of the collector has enhancement of 5-10% with the double pass air flow. A computer model (Wijeysundera, Ah, & Tjioe, 1982) was prepared to validate the experimental results which obtained by (Satcunanathan & Deonarine, 1973). A mathematical model was developed by Al Mahdi and Al Baharna (Al Mahdi & Al Baharna, 1991) to estimate the thermal performance of an n-pass SAH. The results show that by increasing the number of air passes to three, a significant improvement is achieved in the thermal performance of the collector. Ho et al. (Chii Dong Ho, Chang, Lin, Chao, & Tien, 2016) conducted an experimental and theoretical investigation on a double-pass SAH with wire mesh packed in lower channel. The experimental results were compared to the single-pass, flat-plate double-pass and recycling double-pass wire mesh packed. It is observed that by increasing recycle ratio (R) from 0 to 2, the thermal performance is increased. Also, the thermal efficiency of the recycling double-pass wire mesh packed SAH is much higher than that the other SAHs. Demirel and S. Kunc (Demirel & Kunc, 1987) experimentally showed that the thermal efficiency increases by passing the air flow underneath the absorber plate and packed with Rasching rings made of hard plastic. A novel design was proposed by Esen (Esen, 2008) to increase the surface area by arranging obstacles over and under the absorber plate on a double flow SAH. The thermal performance of SAH with obstacles was higher than the SAH without obstacles. Yeh

et al. (H. M. Yeh, Ho, & Hou, 1999) experimentally showed an enhancement of the thermal performance of a SAH with double air passes; simultaneously flows upper and under the absorber plate, in comparison to the conventional collector. Varun and Siddhartha (Varun & Siddhartha, 2010) showed that the maximum thermal efficiency was obtained 75.21% for the collector with three glass covers and the maximum Re of 20000 while the temperature raise was minimum as 3.64℃.

2.1.1.2 Absorber Plate

Air has low capability to gain energy from the absorber plate due its high thermal resistance. The heat transfer of the collector to air can be improved by increasing the heat transfer coefficient. Inducing turbulence in the flow, significantly improve the heat transfer coefficient and subsequently improve the thermal performance of collector. The turbulence can be supplied either by inserting fins in the air flow passage or by inserting a matrix in the flow passage of the collector.

Karmare and Tikekar (Karmare & Tikekar, 2009) obtained the maximum thermal efficiency of 75% for the roughened SAH with metal rib grits at the e/D and Re of 0.035 and 17030, respectively. Baritto and Bracamonte (Baritto & Bracamonte, 2012) developed a mathematical model for no isothermal SAH and solved in non-dimensional form for various design parameters. An equation proposed to calculate the outlet temperature and it shows good agreement with experimental results.

As a survey, some experimental investigations on GSAH are illustrated in Tables (2.1-2.2). Table 2.3 shows the effect of dimensionless parameters on the thermal performance of collector.

Table 2. 1: Different flow patterns and absorber plate configurations with their results on glazed solar air heater.

Authors	Flow Shape and Cover configuration	Absorber Plate Configuration	Results
El-Sebaii et al. (El-Sebaii, Aboul-Enein, Ramadan, Shalaby, & Moharram, 2011)	Double pass	V-corrugated	η increased by 11-14%
C. D. Ho et al. 2009(C. D. Ho, Yeh, Cheng, Chen, & Wang, 2009)	Double pass	Baffled and attached fin	η increased with mass flow rate
Akpinar and Koçyiĝit (Akpinar & Koçyiĝit, 2010; Akpinar & Koçyiğit, 2010)	Single flow	With triangular, leaf shaped and rectangular with 45°obstacles	The highest and lowest η was obtained for leaf shaped and without obstacles, respectively
El-Sebaii and Al-Snani (El-Sebaii & Al-Snani, 2010)	Single pass	Several selective coating material on the absorber plate	The best η was obtained with Nickel–Tin(Ni-Sn) of 46%
Chii Dong Ho et al (Chii Dong Ho, Chang, Wang, & Lin, 2012)	Double pass with various recycling rations	With fins and baffles on the absorber plate	Maximum η was 70%, optimal recycling ratio was 0.5
Sabzpooshani, Mohammadi, and Khorasanizadeh (Sabzpooshani, Mohammadi, & Khorasanizadeh, 2014)	Single pass	Combination of fins and baffles at various arrangements	For $\dot{m} \geq 0.01$, the exergy will decrease inverse of η due to increasing pressure drop inside the collecter

Gupta and Kaushik (Gupta & Kaushik, 2009)	Single pass	Several shapes of roughness on absorber plate	The highest η belongs to circular ribs and V shaped ribs
Bahrehmand, Ameri, and Gholampour (Bahrehmand, Ameri, & Gholampour, 2015)	With/without thin metal sheet in duct and single and double glazed	Rectangular and triangular fins on the absorber plate	The best η was obtained for the collector with fin and thin metal sheet
Hu et al(Hu, Sun, Xu, & Li, 2013)	Single pass	Internal baffles on the absorber plate	The optimal number of baffles was found to be three
Chii Dong Ho, Yeh, and Chen 2011(Chii Dong Ho, Yeh, & Chen, 2011)	Double pass with recycling	Fins attached on the upper part of absorber plate	η increases by increasing the $\dot{m}$ and highest was 80 %
Khas (Indrajit, Bansal, & Garg, 1985)	Single pass	With and without fins on the absorber plate	The collector with fins was more efficient
Priyam and Chand (Priyam & Chand, 2016)	Single pass	Wavy finned absorber plate	The highest η was 63% at the highest $\dot{m}$of 0.0834 kg/s
Sun, Ji, and He (Sun, Ji, & He, 2010)	Single and double pass	Absorber plate was embedded inside the duct	Optimal channel depth was 10 mm and the depth atio of upper channel to lower channel should be more than 1
Flores-Irigollen et al (Flores-Irigollen, Fernández, Rubio-	Inflatable-tunnel	Filled by pebble layer on the absorber plate	Numerical results validated by experimental results

Cerda, & Poujol, 2004)			
ÇAĞLAYAN, ALTA, and ERTEKİN (Caglayan, Alta, & Ertekin, 2014)	Single pass	Absorber plate made by Aluminum (Al) and Cooper (Cu) and several shape	The highest η of (AL) and CU was obtained at the V-shaped and Wavy-shaped respectively as 46.63% and 47.18%
Mohamad (Mohamad, 1997)	A counter-flow and double glazed	With a porous matrix on the absorber plate	η exceeds 75%, having high pressure drop was the disadvantages
Yang et al (Yang, Yang, Li, Wang, & Wang, 2014)	Single flow	Having offset rectangular fins on the absorber	η exceeds 40% even at lowest $\dot{m}$ of 100 m^3/hr
Bayrak, Oztop, and Hepbasli (Bayrak, Oztop, & Hepbasli, 2013)	Single flow	Closed-cell aluminum foams, arranged in in-lined and staggered arrangements	The best η was obtained in the staggered arrangements with the thickness of 6 mm
Sharma, Rizzi, and Garg (Sharma, Rizzi, & Garg, 1991)	Single flow	Employing iron filing on the absorber plate	Improved η by 20%
Mittal and Varshney (Mittal & Varshney, 2006)	Single pass	Packed with wire screen matrix	η increased with packed configuration compared to conventional, Also pressure drop inside collector increased
Dhiman et al (Dhiman, Thakur, Kumar, & Singh, 2011)	Parallel flow	Upper channel packed	η had enhancement of 10-20% compared to conventional collector
El-khawajah et al (El-khawajah, Aldabbagh, & Egelioglu, 2011)	Double pass	Instead of absorber plate, filled by wire mesh between two and four fins	The best η was 85.9% with four fins

Prasad et al (Prasad, Saini, & Singh, 2009)	Single pass	Wire mesh as packing material on the absorber plate	η was varied between 53.3% and 68.5%
Dhiman et al (Dhiman, Thakur, & Chauhan, 2012)	Parallel and counter flow pass	Filled by wire matrix underside of absorber plate	Thermal performance of counter flow was 11-17% higher compared to parallel flow
Aldabbagh et al (Aldabbagh, Egelioglu, & Ilkan, 2010)	Single and double pass	With wire mesh inside the collector	The maximum η and ΔT was 84% and 37℃ at double pass
Sugantharaj et al (Sugantharaj, Vijay, & Kulundaivel, 2016)	Double pass	With and without wire mesh on lower channel	The highest η was 79/8% with wire mesh
C.-D. Ho et al (C.-D. Ho, Lin, Yang, & Chao, 2014)	Double pass and double glazed	With wire mesh and recycling	The maximum η was 68% at the R=2
Chouksey and Sharma (Chouksey & Sharma, 2016)	Single pass	With blacend wire screen matrics	There was good agreement between the experimental and numerical results
Omojaro and Aldabbagh (Omojaro & Aldabbagh, 2010)	Single and double pass	With fins and steel wire mesh instead of absorber plate	The η of double pass was found to be more than single pass by 7-19.4%
Mahmood et al (Mahmood, Aldabbagh, & Egelioglu, 2015)	Single and double pass	Having fins and packed with wire mesh on the absorber plate	The highest η and ΔT was obtained 62.5% and 45.3℃ on double flow

Table 2. 2: Different designs ducts of glazed solar air heater.

Authors	**Characteristics of geometry**	**Dimensionless Parameter**
A. Kumar et al. (Anil Kumar,	Multi V-rib with gap roughness	Re = 2000-20000; P/e = 10;

Saini, & Saini, 2012)		e/D = 0.043; W/w = 6 and α = 60°
S. Yadav et al. (S. Yadav, Kaushal, Varun, & Siddhartha, 2013)	Circular protrusions arranged in angular arc fashion	Re = 3600-18000; P/e = 12-14; e/D = 0.015-0.03; ∅ = 45-75°
S. Skullong et al. (Skullong, Promvonge, Thianpong, & Pimsarn, 2016)	Wavy-groove and delta-wing vortex generator	Delta-wing: width = 20 mm; height = 20 mm have a hole inside with diameter of 3, 5, 7 mm; P_t = 2 H and P_s = H
A. Layek et al. (Layek, Saini, & Solanki, 2007)	repeated transverse chamfered rib–groove	p/e = 4, 5, 6, 7, 8 and 10; e/D_h = 0.022, 0.03, 0.0385 and 0.04; ∅ = 5-30°
A. R. Jaurker et al. (Jaurker, Saini, & Gandhi, 2006)	Rib-grooved	Re = 3000-21000; P/e = 4.5–10.0; e/D = 0.0181–0.0363; g/p = 0.3-0.7
N. S. Deo et al. (Deo, Chander, & Saini, 2016)	Multi-gap V-down rib combined with staggered ribs	Re = 4000-12000; P/e = 4–12; e/D = 0.026–0.057 and α = 40-80°
A. Bekele et al. (Bekele, Mishra, & Dutta, 2014)	Delta-shaped obstacles	Re = 2100–37450; e/H = 0.25; 0.50 and 0.75; p_l/e = 11/2, 7/2 and 3/2; α = 30°, 60° and 90°
V. S. Hans et al. (Hans, Saini, & Saini, 2010)	Multiple v-rib roughness	Re = 2000 to 20000; P/e = 6–12; e/D = 0.019–0.043; W/w = 1–10 and α = 30–75°
A. Lanjewar et al. (Atul Lanjewar, Bhagoria, & Sarviya, 2011)	W-shaped rib roughness	Re = 2300 -14,000; p/e = 10; e/D_h = 0.018-0.03375; W/H = 8.0; α = 30-75°
S. Singh et al. (S. Singh,	V-down rib roughness	Re = 3000-30000; p/e = 4-12; e/D_h = 0.015-0.043; α =

Chander, & Saini, 2012a)		30-75°
S. B. Bopche et al. (Bopche & Tandale, 2009)	U-shaped turbulators	Re = 3800-18000; p/e = 6.67-57.14; e/D_h = 0.0186-0.03986; α = 90°
P. Promvonge et al. (Promvonge, Khanoknaiyakarn, Kwankaomeng, & Thianpong, 2011)	Combination of triangular rib and delta-winglet turbulators	Re = 5000-22,000; P_t/H = 1.0; P_l/H= 1.33; e/H = 0.2; α = 30°, 45° and 60°
M. M. Sahu et al. (Sahu & Bhagoria, 2005)	90° broken transverse ribs	Re = 3000-12,000; pitch of ribs = 10–30 mm, roughness height = 1.5 mm
B. Bhushan et al. (Bhushan & Singh, 2012)	Roughened with formation of protrusions	Re = 5000-65000; relative short way length = 18.75-37.5; relative long way length = 25.0–37.5; relative print diameter = 0.147–0.367 and e/D = 0.03
G. Tanda (Tanda, 2011)	45° inclined, continuous, transverse continuous, transverse broken, discrete V-shaped ribs	Re = 4000-20000; p/e = 6.66, 10, 13.33 and 20; e/D = 0.09; e/H = 0.15 and α = 45-60°
S. Tamna et al. (Tamna, Skullong, Thianpong, & Promvonge, 2014)	V-baffle vortex generators in in-line and staggered arrangements	Re = 4000-21,000; relative baffle height= 0.25; baffle pitch to channel-heigh=0.5, 1, and 2; α = 45°
S. Singh et al. (S. Singh, Chander, & Saini, 2015)	V-down rib having gap equal to rib height in both legs of V	Re = 3000-15000; p/e = 4, 6, 8, 10 and 12; e/D_h = 0.043; α = 60°
X. Gao et al. (X. Gao & Sundén, 2001)	Parallel ribs and V-shaped ribs	Re = 1000-6000; p/e = 10; e/D_h = 0.06; α = 60°

R. Karwa (Karwa, 2003)	Repeated ribs in pattern of: transverse, inclined, V-continuous, V-discrete	Re = 2800-15000; p/e = 10; e/D_h = 0.0467-.050; W/w =7.19-7.75; α = 60°
S. Singh et al. (S. Singh, Chander, & Saini, 2012b)	V-down rib having gap	Re = 3000-15000; p/e = 8; e/D_h = 0.043; α = 30-75°
M. K. Mittal et al. (Mittal, Varun, Saini, & Singal, 2007)	Inclined ribs as roughness	Re = 2000-24000; p/e = 10; e/D = 0.02-0.04; α = 60°; ∅ = 10°
R. P. Saini et al. (Saini & Verma, 2008)	Dimple-shape roughness	Re = 2000-12000; p/e = 8-12; e/D = 0.0189 to 0.038
Varun et al. (Varun, Patnaik, Saini, Singal, & Siddhartha, 2009)	Transverse and inclined ribs	Re = 2000-14000; p/e = 3-8; e/D = 0.030
S. Singh et al. (S. Singh, Chander, & Saini, 2011)	Discrete V-down ribs	Re = 3000-15000; p/e = 4-12; e/D = 0.015-0.043; g/e = 0.5-2.0; d/w = 0.20-0.80; α = 30-75°
R. Karwa et al. (Karwa & Chauhan, 2010)	60° v-down discrete rectangular cross-section repeated rib	Re = 1070–26350; L = 1–4 m; H = 5, 10 and 20 mm; e/D_h = 0.02–0.07; α = 0° and 45°
J. L. Bhagoria et al. (Bhagoria, Saini, & Solanki, 2002)	Transverse wedge shaped rib	Re = 3000-18000; $60.17\emptyset^{-1.0264} < p/e > 12.12$; e/D = 0.015–0.033; W/w = 5; ∅ = 8-15°
P. Sriromreun et al. (Sriromreun, Thianpong, & Promvonge, 2012)	Baffle in a zigzag shape turbulators	Re = 3000-15000;p/H = 1.5, 2 and 3; e/H = 0.1, 0.2 and 0.3; α = 45°
S. Skullong et al. (Skullong,	Combined wavy-rib and groove turbulators	Re = 4400-20400; P/H = 0.5, 1 and 2; b/H = 0.25; α =

Kwankaomeng, Thianpong, & Promvonge, 2014)		45°
A. Lanjewar e al. (A. Lanjewar, Bhagoria, & Sarviya, 2011)	W-shaped ribs	Re = 2300-14,000; p/e = 12–24; e/D_h= 0.03375; W/H = 8.0; α = 30-75°
S. Yadav et al. (S. Yadav, Kaushal, Varun, & Siddhartha, 2014)	Arc shape oriented protrusions	Re = 1000–40000; p/e = 12-24; e/D= 0.015–0.030; α = 45–75°
R. Chauhan et al. (Chauhan & Thakur, 2012)	Impinging jet	Re = 3800–16000; X/D_h = 0.435–1.739; Y/D_h= 0.435–0.869; W/Z = 11.6; D_j/D_h= 0.045–0.109
N. K. Pandey et al. (Pandey, Bajpai, & Varun, 2016)	Multiple-arc shaped with gaps	Re = 2100-21000; p/e = 4-16; e/D_h= 0.016–0.044; W/w = 10; g/e = 0.5–2.0; α = 30–75°
V. B. Gawande et al. (Gawande, Dhoble, Zodpe, & Chamoli, 2016b)	Reversed L-shaped ribs	Re = 3800–18000; p/e = 7.14-17.86; e/D= 0.042; W/H = 5
S. Kumar et al. (S. Kumar & Saini, 2009)	Thin circular wire in arc shaped	Re = 6000–18,000; p/e = 10; e/D= 0.0299-0.0426; W/H = 12; α = 30-60°
D. Jin et al. (Jin, Zhang, Wang, & Xu, 2015)	Multi V-shaped ribs	Re = 8000-20000; p/e = 2, 5, 7, 10 and 20; e/D= 0.025-0.115; W/w = 1-10; α = 30-75°
A. Acir et al. (Acir, Ata, & Canli, 2016)	Circular ring turbulators	Re = 3000 –21000; p/H = 2, 2.8 and 3.5; hole diameter = 8 mm;
A. S. Yadav et al. (A. S. Yadav	Equilateral triangular sectioned rib	Re = 3800-18000; p/e = 7.14-35.71; e/D= 0.021-0.042;

& Bhagoria, 2014)		W/H = 5.0
V. B. Gawande et al. (Gawande, Dhoble, Zodpe, & Chamoli, 2016a)	20° angled rib	Re = 2000-18000; p/e = 7.14, 10.71, 14.29 and 17.80; e/D= 0.042; W/H = 5.0; α = 0-40°
V. B. Gawande et al. (Gawande, Dhoble, & Zodpe, 2014)	Circular transverse ribs	Re = 3800–18000; p/e = 10-25; e/D_h= 0.015–0.03; W/H = 5.0
A. Singh et al. (A. Singh & Bhagoria, 2014)	Repeated transverse square sectioned rib	Re = 3800–18000; p/e = 7.14-35.71; e/D= 0.021-0.042
T. Rajaseenivasan et al. (Rajaseenivasan, Srinivasan, & Srithar, 2015)	Circular tubes having V-shape inside	Re = 6000-12000
S. Singh et al. (S. Singh, Singh, Hans, & Gill, 2015)	Repeated transverse ribs	Re = 3000-15000; p/e
T. Alam et al. (Alam & Kim, 2016)	Semi elliptical shape obstacles placed in V-down shape in-line and staggered arrangements	Re = 6000-18000; longitudinal pitch ratio = 3.5; transverse pitch ratio = 2.33; α = 30–90°
A. S. Yadav et al. (A. S. Yadav & Bhagoria, 2013)	Circular transverse wire rib	Re = 3800-18000; p/e = 7.14-35.71; e/D= 0.021-0.042; W/H = 5.0
S. V. Karmare et al. (Karmare & Tikekar, 2010)	Metal grit ribs at circular, triangular and square shapes as roughness	Re = 3600-17000; p/e = 17.5; e/D_h= 0.044; α = 60°
M. Sethi et al. (Sethi, Varun, & Thakur, 2012)	Dimple shaped elements arranged in angular fashion (arc)	Re = 3600-18000; p/e = 10–20; e/D_h= 0.021–0.036; W/H = 11; α = 45–75°

A. Kumar et al. (Arvind Kumar, Bhagoria, & Sarviya, 2009)	Discrete W-shaped ribs	Re = 3000-15000; p/e = 10; e/D_h= 0.0168-0.0338; W/H = 8; α = 30-75°
A.-M. E. Momin et al. (Momin, Saini, & Solanki, 2001)	V-shaped rib	Re = 2500-18000; p/e = 10; e/D_h= 0.02–0.034; W/H = 10.15; α = 30–90°
A. Layek et al. (Layek, Saini, & Solanki, 2009)	Combination of 60° V-groove and chamfered ribs	Re = 3000-21000; p/e = 10; e/D_h= 0.03; ∅ = 5-30°
E. A. Handoyo et al. (Handoyo, Ichsani, Prabowo, & Sutardi, 2016)	Delta-shaped obstacles on the V-corrugated absorber plate	Re = 3600-17000; p_l/e = 1.5; e/H= 0.5-0.75; α = 60°

Table 2. 3:Effects of different parameters on the thermal performance of GSAH.

p/e	f and Nu both increase with relative roughness pitch for constant p/e
e/D	f and Nu both increases with increase of e/D
$\emptyset$	f and Nu both increases with Stanton number at increasing the chamfer angle
Inclination of ribs	The amount of heat transfer rate to air flow increases
Area	The heat transfer rate is the highest at 60°

2.1.2 Unglazed Solar air Heater

While the above-mentioned studies concentrate on improving the thermal efficiency of GSAH, the aspect of maximum heat loss occurring from the glazing cover is overlooked. To counter this problem, preheating the inlet air from the unglazed perforated plate in the unglazed transpired collector (UTC) is proposed. UTCs have emerged as a simple yet efficient technology. A flat transpired SAH comprises of an unglazed perforated absorbing plate. The heat transfer to air flow in the substrate is drawn through a fan via several small perforations.

The concept of UTC was developed in the late 1990s by Christensen et al (Christensen, C, Hancock, E, Barker, G, Kutscher, n.d.). The results of their experiments indicated that the UTC achieves 70% cost reduction compared to the GUCs. Kutscher et al (Kutscher, Christensen, & Barker, 1993) indicated that perforating the cover plate permits the ventilation air to gather heat lost by convection and radiation at its surface. Gunnewiek et al. investigate theoretically the effect of with (Gunnewiek, Hollands, & Brundrett, 2002) and without (Gunnewiek, Brundrett, & Hollands, 1996) the wind velocity on the thermal performance of the UTC. Results indicated that reverse flow is observed at a mass flow rate of less than 0.0125 kg/s, hence mass flow rates equal to this and lower should be avoided.

Further, the code is modified by considering the effect of wind velocity on the flow distribution of an unglazed transpired plate. Christensen et al. (Christensen, Craig B, Charles F. Kutscher, M. Gawlik, 1997) experimentally investigated the effect of two different materials of absorber plates of two UTCs having the same thickness, aluminum, and styrene plastic. At low mass flow rates of up to 0.02 kg/s, the heat transfer from the plastic absorber plate to the air stream increases by 20% compared to the aluminum plate. Hollick (Hollick, 1999) shows that UTC performs reasonably well when connected to a dryer compared to when the dryer is heated by oil. In this numerical model, the most effective collector heat exchange was obtained at 80% for a perforation diameter being 0.8 mm and pitch 0.12 mm. Fleck et al. (Fleck, Meier, & Matovic, 2002) indicate that the highest efficiency cannot be achieved at low wind speeds. The effects of the thickness of the absorber plate, pitch between the holes and diameter of the perforations were studied by Børvik et al. (Børvik, Hopperstad, Berstad, & Langseth, 2002). The highest thermal efficiency is obtained 77.64% at the black colored UTC by Gao et al. (L. Gao, Bai, Fang, & Wang, 2013). It is found that UTCs are both aesthetically and financially better compared to conventional SAHs. Vaziri et al. (Vaziri, Ilkan, & Egelioglu, 2015) experimentally conducted the effect of different colors of a perforated glazed collector. The results indicated that the maximum thermal efficiency was obtained 85% for black. Croitoru et al. (Croitoru, Nastase, Bode, & Meslem, 2016) indicated that the amount of heat transferred from cross perforation to air increases 40% in comparison to conventional UTC (having round perforation shape). Dymond and Kutscher et al. (Dymond & Kutscher, 1997) proposed a numerical model which can be utilized as a tool for designing and calculating the thermal performance of UTC.

A CFD model was developed to examine the heat transfer and flow characteristics of a UTC by Arulanandam et al. (Arulanandam, Hollands, & Brundrett, 1999). The numerical domain of perforated plate is divided into three sections, as proposed by Kutscher (Kutscher, 1992). This study modifies the Kutscher model by introducing the back surface as an adiabatic surface. The results of the front and hole regions are in good agreement (within 1%) with the Kutscher model. Moreover, the results demonstrate that employing low conductivity materials, such as plastics, yields acceptable efficiencies. The results of a mathematical study by Van Decker et al. (Van Decker, Hollands, & Brunger, 2001) on heat exchange effectiveness of a UTC demonstrated that the maximum percentage rise in temperature of the perforated plate is 62%, 28%, and10%, respectively, for the front surface, hole, and back side of the cover plate. Gawlik et al. (Gawlik, Christensen, & Kutscher, 2005) figured out the effect of the conductivity of unglazed plate is small on the performance of UTC. The results of a mathematical model investigated by Leon and Kumar (Leon & Kumar, 2007) indicated that the maximum effective collector heat exchange was obtained 80% for a perforation diameter being 0.8 mm and pitch 0.12 mm. Also, the highest thermal efficiency achieved is 65% for the highest mass flow rate and solar radiation. The predicted results obtained by Badache and Hallé (Badache M, Hallé S, 2012) indicated that the effect of hole diameter is not significant on the thermal performance compared to solar irradiation and mass flow rate. The effect of bed height on the thermal efficiency of UTC is studied experimentally and numerically by Badache et al. (Badache, Rousse, Hallé, & Quesada, 2013). It was found that the maximum heat transfer takes place at the front surface and minimum at the back of perforated plate. The experimental and CFD simulation results are in good agreement. In addition, the maximum thermal efficiency difference between the two

plenum thicknesses (5 and 15 cm) is only 3.25. The results of a numerical study on UTC with courrogated plate by Collins and Abulkhair (Collins & Abulkhair, 2014) indicated that wind velocity has not significant effect on the thermal performance of UTC. Gao et al. (L. Gao, Bai, & Wu, 2013) numerically studied and indicated that the effect of hole pitch and hole diameter on heat transfer in UTC are significant and slight, respectively. Vasan and Stathopoulos (Vasan & Stathopoulos, 2014) investigated experimentally and numerically a UTC, with a uniform wind speed distribution, the coefficients of effectiveness and convective heat transfer were 50% and 20%, respectively, (overestimate and underestimate) compared to the actual wind distribution. A numerical model was proposed and verified experimentally by Rad and Ameri (Rad & Ameri, 2016)(Rad & Ameri, 2016) for an unglazed transpired collector-2stage (UTC-2stage). The first stage is a UTC and the second one is an inclined transpired collector with a transparent cover. The heat transfer and flow coefficients were calculated both experimentally and numerically on the GTC with slit perforation instead of round perforation. The results predicted with the numerical model by li et al. (Li, Li, & Li, 2016) were validated by Kutscher, which indicated that the effective efficiency is 64% and 40%, respectively, at the minimum and maximum volume flow rates. This number increases by increasing volume flow rate up to 160 m^3/hr and decreases thereafter up to the highest mas flow rate. Also, the effective efficiency improves with increases in the ambient temperature and perforation diameter, and decreases in the pitch, plenum thickness and ambient temperature.

The main disadvantage of UTC is the unglazed perforation cover, which leads to greater heat convection losses. Therefore, using a glazed material as cover plate is the most suitable to decrease heat losses from the cover plate. High cost and fast

deterioration of plastic cover (as Plexiglas) compared to glass make the glass the best option for the cover plate. The deviation from a numerical results and experimental results of glazed transpired collector was obtained 3.6% by Zheng et al. (Zheng et al., 2016).

A novel design of back-pass non-perforated unglazed SAH fabricated in large scale and was investigated experimentally by Paya-Marin et al. (Paya-Marin, Lim, Chen, Lawson, & Gupta, 2015). Results show that the length of the collector cavities has a direct impact on the efficiency of the system. It is found that wind speeds of up to 4 m/s across the collector has not significant effect on the thermal performance of the collector. Also, the performance of the system is not sufficient changed by increasing mass flow rate for beyond a height-to-flow ratio of 0.023 $m/m^3/hr/m^2$.

To obtain the key factors affecting the ability of a glazed balcony, the temperatures on 22 balconies (17 glazed) and adjacent flats were monitored by Hilliaho et al. (Hilliaho, Köliö, Pakkala, Lahdensivu, & Vinha, 2016). The monitored data showed that the temperature of both glazed and unglazed balconies were higher than the ambient temperature. The temperatures of unglazed balconies were 2℃ and those of glazed balconies 5℃ higher than the outdoor air temperature. Also, The three key factors affecting the glazed balcony temperatures seemed to be the level of air leakage in the balcony vertical structures, the balcony's ability to capture solar radiation, and the heat gain from an adjacent flat, in that order. A mathematical model was developed by Gao et al. (L. Gao, Bai, & Mao, 2014) to assess the potential for glazed transpired collectors (GTC) using recirculated air. The results indicate that decreasing the porosity by 100% led the thermal efficiency and temperature rise to have enhancement of 56% and 35%, respectively. The thermal

efficiency and temperature rise of UTC were found 70.82% and 23.47℃ respectively, while, the corresponding values of the flat plate collector were found 43.09% and 14.28℃, respectively. Also, the exit air temperature of GTC is increased considerably by the use of recirculated air.

2.2 Applications of SAH

During the last decades, many efforts have been conducted to integrate SAH with PV systems and employing storage material. The main purpose is to improve the performance of the systems and reduce the cost of them by combining with the SAH. The thermal efficiency of PV is varied from 6 and 12 and the most of the remaining energy, which is not recovered, is thermal energy. From the literature review, it seems that the thermal efficiency of SAH is in the range of 30-85%. During last decades many effort have been conducted to develop PV-SAH project to provide both thermal and electrical energy. At the hybrid system, The PV cells are cooled by the air flow, which increases their conversion efficiency and the heated air is captured and utilized.

The concept of PV/T system was proposed by Kern et al. (E. C. Kern & Russell, 1978). A hybrid collector consists of three PV modules which were encompassed by of 36 solar cells was investigated numerically and experimentally by Solanki et al. (Solanki, Dubey, & Tiwari, 2009). The thermal, electrical and overall efficiency of the solar heater was obtained 42%, 8.4%, and 50%, respectively. An experimental study was investigated by Hollick (Hollick, 1998) to investigate the method of integrating photovoltaic cells with the transpired SAH, manufactured prototypes, measured the combined electrical and thermal energies produced and compared the results with single function reference panels. Adding thermal energy can increase the

total solar combined efficiency to over 50% with little or no increase in capital cost. In addition, the results indicated that the temperature of the PV cells with the combined PV SOLARWALL and only PV was 36℃ and 45℃, respectively.

Thermal energy could be stored, in general, in the form of either sensible or latent heat. From an energy storage point of view, latent heat thermal storage is an efficient and suitable heat storage means and has the advantages of large thermal capacity with constant storage (melting) temperature. The absorber plate of a conventional SAH is replaced by two different configurations of tubes as straight set of tubes and corrugated set of tubes by Fath (Fath, 1995). The daily average heater efficiency for without filled storage material for the corrugated set of tubes the straight set of tubes conventional fiat plate absorber is 59% , 53%, and 38.7%, respectively. By filing the thermal energy storage material in set of tubes with sensible heat (sand) and two latent heat (paraffin wax and Glauber's salt), results demonstrated an increment is obtained on the thermal efficiency of the SAH with paraffin wax (63.35%) and with sand (59%). An experimental study on the SAH with Granular Carbon as the storage material by Saxena et al. (Saxena, Agarwal, & Srivastava, 2013) showed that the highest thermal efficiency of natural and forced convection flow is 18.6% and 73.65%, respectively. An analytical and experimental investigation was conducted by Bouadila et al. (Bouadila, Kooli, Lazaar, Skouri, & Farhat, 2013) on a SAH with latent storage collector employing spherical capsules as a packed bed absorber. The results demonstrated that the useful energy that can be utilized during 11 hours of off -sun time was 200 W/m^2. In addition, the daily energy efficiency varied between 32% and 45%.

To the best of our knowledge, no experiments have been performed with the slit glazed solar air heater (SGSAH). The main aim of this investigation were to determine the effect of different gap distances between the glazed slits and bed heights of the collector on the thermal performance by varying the air mass flow rates. In the SGSAH system, air is pre-heated by passing through slit glazed similar to as in the perforated glazed in the UTC. With this new design of SAH, advantages of both GUC and UTC can be combined, i.e., having glass as the glazed cover and slit glazed as semi-transpired, respectively, thereby improving the performance of SAHs.

Chapter 3

EXPERIMENTAL SETUP DESCRIPTION

SAH is a converter of solar energy to thermal energy which can be utilized in many applications to reduce CO_2 emissions globally as discussed in the previous chapter. Typically, SAH consists of absorber plate, air duct, cover plate and fan (in the active systems). As mentioned in previous chapters, numerous studies have been conducted to improve the thermal performance of SAHs by modifying the conventional SAH. In this chapter, the construction and set ups of the present study are introduced.

3. 1 Configurations of the Modified SAH

Thermal performance of the new modified SAH is investigated in various configurations on three series as shown in Table 3.1.

Table 3. 1: Configurations of various series of experimental processes.

Number of series	Number of apparatus	Bed height (cm)	Slit width/Pitch (cm)	Gap distance/Hole diameter (mm)	Mass flow rate (kg/s)
Series I	Three SGSAH	7, 5, and 3	6	0.5, 1, 2, and 3	0.014, 0.022, 0.029, 0.036, 0.043, 0.050, and 0.057
Series II	Three SGSAH	7	6, 5, and 4	0.5, 1, 2, and 3	0.014, 0.022, and 0.029
Series III	One SGSAH + One UTC	7	3	3	0.014, 0.022, and 0.029

The main parameters utilized in each set up are the bed height, gap distance, unglazed perforated cover plate, and slit width. The schematic of constructed SGSAH is presented in Fig. 3.1. Figure 3.2 shows the pictorial view of the three SGSAHs constructed for this study.

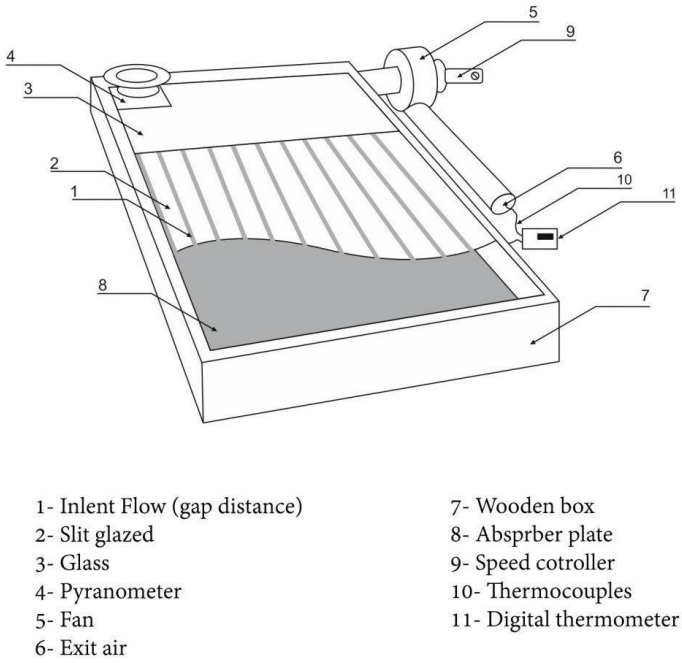

Figure 3. 1:Schematic view of the slit glazed collector system.

Figure 3. 2:Pictorial view of the experimental setup of three slit glazed solar air heaters.

3.2 Experimental Setup

In this study, three SGSAHs and a UTC were constructed to investigate the thermal performance. The frames of the collectors were made from plywood with length, width and thickness 154 cm, 91 cm and 1.5 cm, respectively, and painted in matt black. The bed heights of three SGSAHs were 3 cm, 5 cm, and 7 cm. The absorber plate of the SGSAH and unglazed perforated cover of UTC was made of 1 mm thick of low carbon steel metal sheet and painted in matt black. The bed height of UTC was 7 cm. The cover plate of UTC has 3 mm diameter holes and area of 1.01 ×0.95 m^2. In addition, the centre to centre distance between holes of perforated sheet was 3 mm see Fig. 3.3.

Normal window glass panes, 4 mm in thickness, were used as glazing cover at SGSAH with length and width of each pane being 131 cm and 6 cm (latter 5 cm and 4 cm) respectively. In order to reduce heat losses from the collectors, the sides and bottom of the collectors were insulated by 3 cm thick Styrofoam. A 4 mm thick glass, 91 cm wide and 23 cm long, was placed at the top of the collector to ensure uniformity in flow and to prevent any flow reversals. The experiments were conducted for four different gaps between the panes, viz., 0.5 mm, 1.0 mm, 2.0 mm, and 3mm, and mass flow rates for the series I of experiments were chosen to be 0.014, 0.022, 0.029, 0.036, 0.043, 0.050, and 0.057 (kg/s). Also, mass flow rates of series II and series III of experiments were 0.017, 0.022, and 0.029 (kg/s).

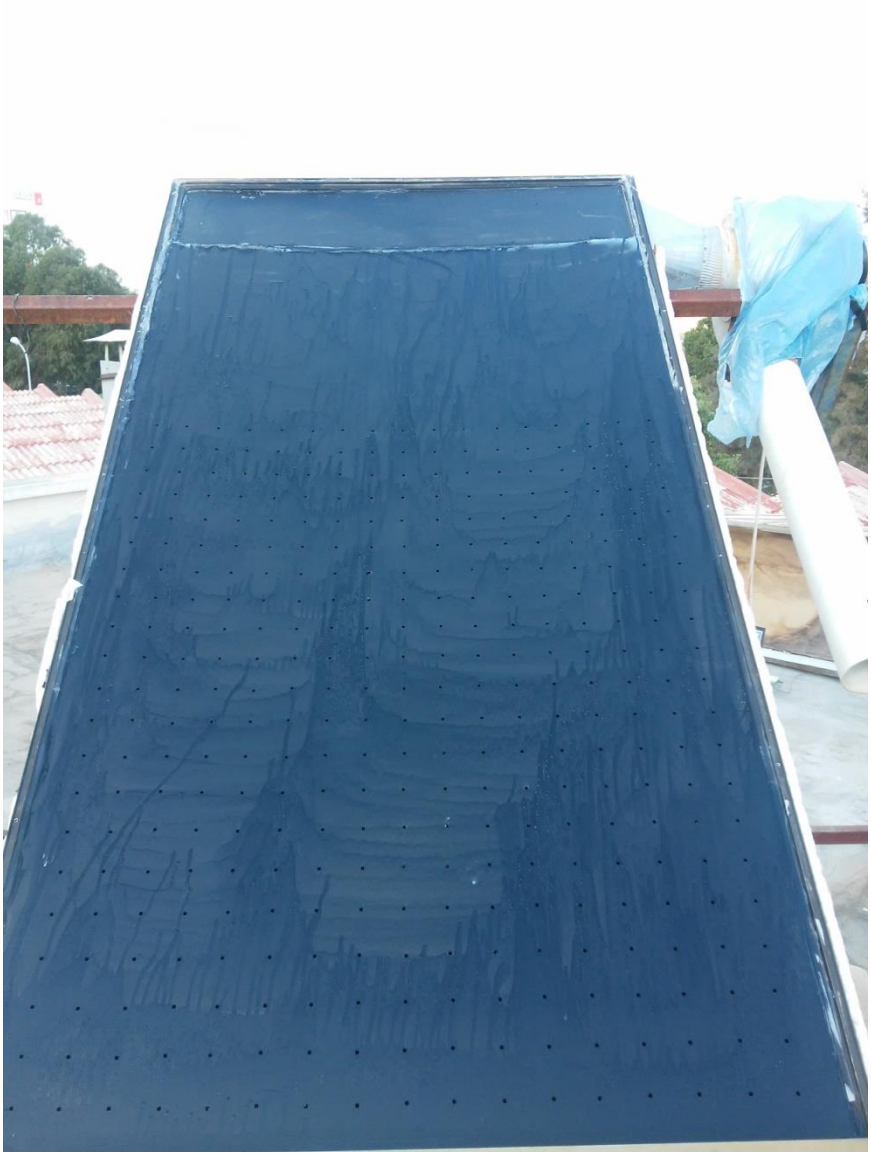

Figure 3. 3:Perforated cover plate of UTC.

3.2 Experimental Measurements

The equipment employed in this study are briefly presented in the following subsections.

3.2.1 Pyranometer

Solar intensity was measured by using an Eppley Radiometer Pyranometer (PSP) with a solar radiation meter model HHM1A digital Omega with 0.25% basic DC accuracy and a resolution of ±0.5% having a range of 0 to 2800 W/m^2. Figure 3.5

shows the PSP connected to voltmeter. To achieved the maximum solar irradiation on the collectors, collectors were placed toward south and their inclined angle were fixed at 39.5° due to the geographical location of Cyprus (35.125 °N and 33.95 °E longitude).

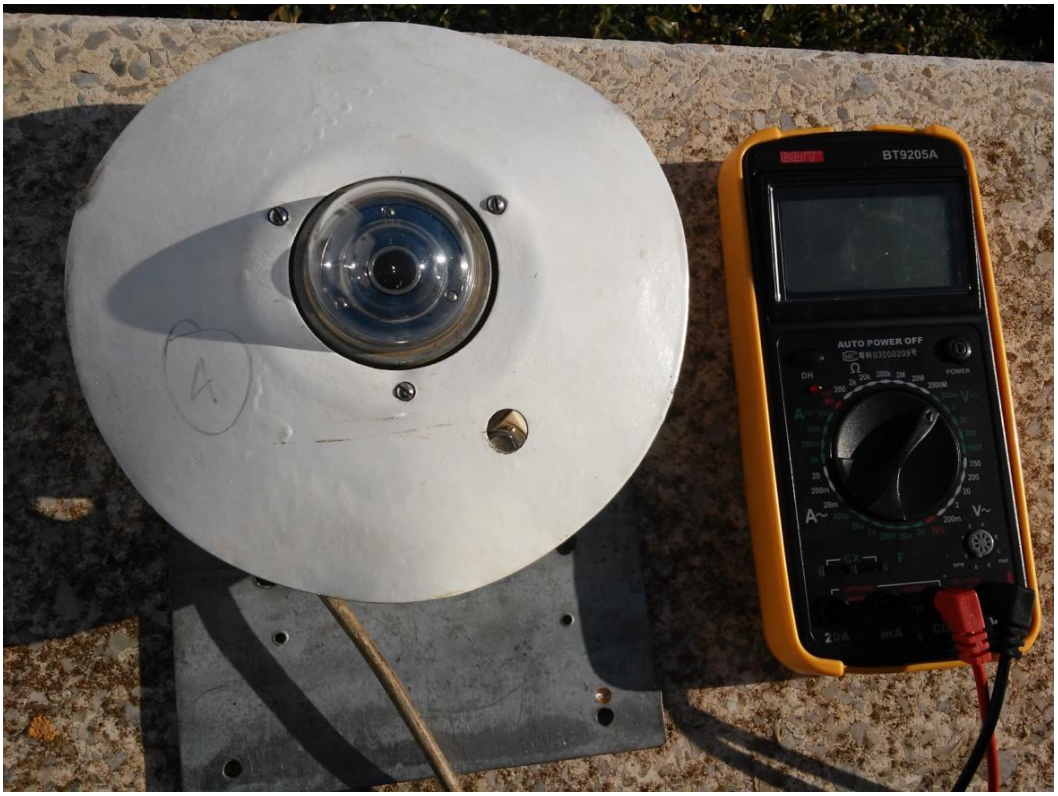

Figure 3. 4:Eppley Radiometer Pyranometer connected with HHM1A.

3.2.2 Thermometer and Thermocouples

For each SGSAH, two type-K thermocouples were employed to measure the inlet and outlet air temperature and the temperature at different points on the glazing. Two-channel digital thermometers with an accuracy of ±0.5°C were used to measure temperatures hourly during the day (Fig 3. 5).

Figure 3. 5:Two-channel digital Thermometer with Thermocouples.

3.2.3 Air velocity

The air velocity was measured using an Extech 407112 Vane anemometer. For the range 0.4–10 m/s, the reading accuracy and data resolution were 0.2 m/s ±2% and 0.01 m/s, respectively. A dimmer switch was used to control the air flow rate for each collector. The pictorial view of the anemometer is presented in Fig. 3.6.

Figure 3. 6:The Extech 407112
Vane Anemometer.

3.3 Uncertainty evaluation

In this section, the uncertainty of the air mass flow rate and thermal efficiency are presented. The mass flow rate is determined as:

$$\dot{m} = \rho A V \tag{3.1}$$

Where, ρ is the density of air, V is the outlet air velocity and A is the cross-sectional area of the outlet. The fractional uncertainty, $\frac{\omega_{\dot{m}}}{\dot{m}}$, for the air mass flow rate can be calculated as (Holman, 1989):

$$\frac{\omega_{\dot{m}}}{\dot{m}} = \left[\left(\frac{\omega_{T_{air}}}{T_{air}}\right)^2 + \left(\frac{\omega_V}{V}\right)^2 + 4\left(\frac{\omega_r}{r}\right)^2 \right]^{1/2} \tag{3.2}$$

Where, T_{air} is the average temperature between the inlet and outlet,ω_r r is the uncertainty of the pipe radius of air outlet, $\omega_{T_{air}}$is the uncertainty for the film air temperature, and ω_V is the uncertainty for the velocity.

The fractional uncertainty in the efficiency can be found as:

$$\frac{\omega_\eta}{\eta} = \left[\left(\frac{\omega_{\dot{m}}}{\dot{m}}\right)^2 + \left(\frac{\omega_{\Delta T}}{\Delta T}\right)^2 + \left(\frac{\omega_I}{I}\right)^2\right]^{1/2} \quad (3.3)$$

Where, ω_η, $\omega_{\Delta T}$, and ω_I are the uncertainty of the efficiency, the temperature difference between the inlet and outlet temperature, and solar intensity, respectively.

The mean uncertainties within the mass flow rate and thermal efficiency for the highest air mass flow rate were calculated to be 1.45% and 3.7%, respectively.

3.4 Experimental Procedure

The effect of the bed height was investigated in the first experimental series (series I), the effect of the width of glass pane was investigated in series II, and a comparison between the UTC and SGSAH were investigated in series III. The first experimental series were conducted between May 24, and July 10, 2015. The second experimental series were conducted in November 2015 and the third experimental series were conducted in December 2015. The experiments were conducted during clear sky condition at Famagusta (35.125° N and 33.95° E longitudes) in Cyprus. In addition, it should be mentioned that the part I was carried out from 8.30 am to 4.30 pm while series II and series III were conducted from 7.30 am to 15.30.

Chapter 4

DEVELOPMENT OF A MATHEMATICAL MODEL OF THE SGSAH

The heat transfer of the SGSAH is investigated by considering the energy balance between the slit glazed, stream air and the absorber plate. The convective and radiation heat transfer rates between the components of the collector have been estimated by utilizing the rate equations. The model consists of various empirical relations to estimate the several heat transfer coefficients used in the rate equations.

4.1 The Conservation of Energy Equation on the SGSAH

The assumptions used in developing the analytical model are listed below:

I. The panes and absorber plate temperatures are assumed to be uniform (isothermal) throughout their respective surfaces. While unglazed cover plate are mostly isothermal form hole-to-hole, glazed cover plate shows some non-isothermality. However, investigations by Gawlik et al. (Gawlik et al., 2005) have indicated that non-isothermality does not have major effect on the thermal performance of the collector.

II. Air stream through the panes is assumed homogeneous. While in reality, the profile of air flow could be non-homogenous (especially in collectors having large heights and active) (Gunnewiek et al., 1996), (Dymond & Kutscher, 1997).

III. There is no reversal flow in the slit glazed.

IV. Heat losses from the edge are not significant (Summers DN, Mitchell JW, Klein SA, 1996).

V. The experiments were conducted under steady state conditions.

VI. The air stream is incompressible.

VII. The temperature gradient through the thickness of glass panes is assumed to be zero due low conductivity.

Figure 4.1 illustrates the schematic view of the heat transfer modes and heat transfer exchanges in the collector. Heat losses from the collector are due to radiation and convection losses from the glass panes and absorber plate.

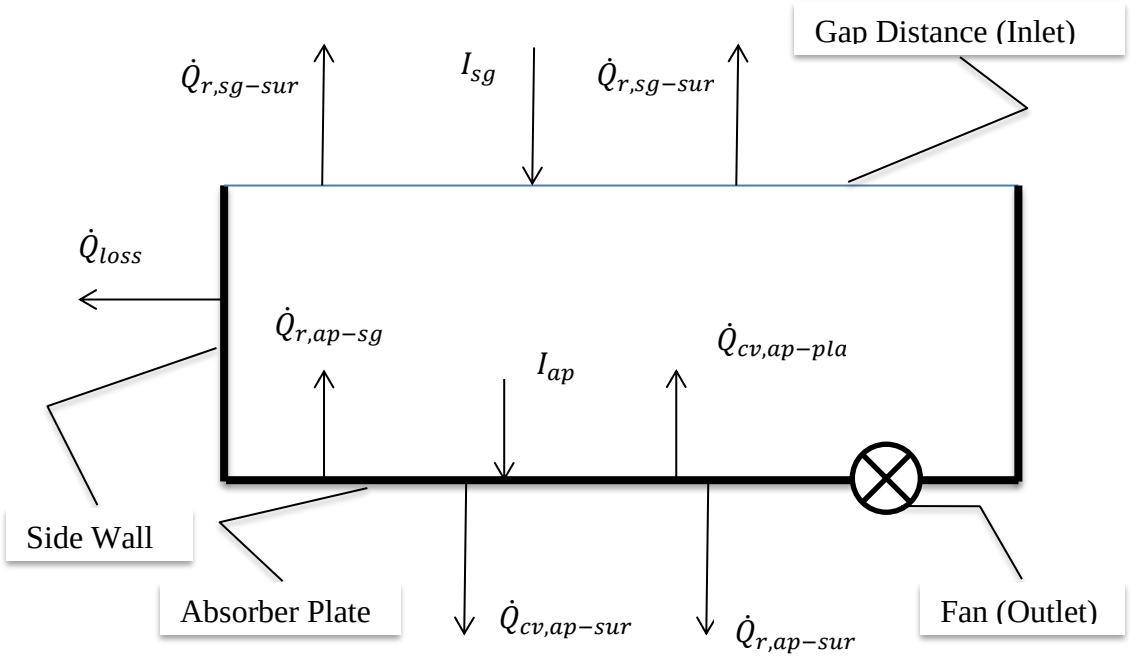

Figure 4. 1: Heat transfer exchanges in SGSAH.

4.2 Energy balance

The solar energy is transmitted through the slit glazed and then absorbed by the absorber plate. Energy balance can be analyzed on the slit glazed, absorber plate, and air flow.

4.2.1 Energy conservation on the glass panes

The energy equation for the glass panes

$$I_{sg} - \dot{Q}_{cv,sg-air} - \dot{Q}_{r,sg-sur} + \dot{Q}_{r,ap-sg} = 0 \quad (4.1)$$

Where $I_{sg} = \alpha_{sg} I A_{sg}$ is the fraction of the solar energy absorbed by slit glazed. The term α_{sg}represents the absorptivity of the slit glazed. The term $\dot{Q}_{cv,sg-air}$ refers the convection heat transfer from slit glazed to air, which includes heat transfer from the slit glazed front, panes and back surface to the plenum air. A part of energy

transferred by radiative from the slit glazed to air ($\dot{Q}_{r,sg-sur}$) and absorbed by slit glazed from absorber plate ($\dot{Q}_{r,ap-sg}$).

4.2.2 The Conservation of Energy on Air Flow on the Plenum

$$\dot{m}_{air}c_p(T_{exit} - T_{in}) - \dot{Q}_{cv,ap-pla} - \dot{Q}_{loss} = 0 \quad (4.2)$$

Where $\dot{Q}_{cv,ap-sg}$ is the heat transferred from absorber plate to air flow inside the plenum. The term T_{exit}refers to the outlet temperature of air at the exit of the slit glazed.

4.2.3 The Energy Balance on the Absorber Plate

$$I_{ap} - \dot{Q}_{cv,ap-pla} - \dot{Q}_{cv,ap-sur} - \dot{Q}_{r,ap-sg} - \dot{Q}_{r,ap-sur} = 0 \quad (4.3)$$

Where $I_{ap} = \alpha_p \tau_{sg} I A_{ap}$is the fraction of solar energy absorbed by the absorber plate. The terms $\tau_{sg}$and α_p are the transmissivity of the slit glazed and absorptivity of the plenum, respectively. The area of absorber plate is represented by A_{ap}. $\dot{Q}_{cv,ap-air}$ gives the convection heat transfer of absorber plate to plenum air inside the collector. Absorber plate emits radiative heat transfer to glass panes and the back (surrounding) by $\dot{Q}_{r,ap-sg}$ and $\dot{Q}_{r,ap-sur}$, respectively.

4.3. Rate Equations

4.3.1. Convective Heat Transfer from Slit Glazed to Air

The convective heat transfer rate is determined using the convection heat transfer coefficient, the temperature difference between the surface and surrounding fluid, and surface area. Heat transfer coefficient is estimated by using the following empirical correlations. Velocity inside the plenum varies from zero at the bottom to highest at the top of collector which causes to use an average velocity at inside the collector. The convective heat coefficient between the slit glazed and ambient air

through the slit glazed is calculated by the following experimental correlation(Summers DN, Mitchell JW, Klein SA, 1996).

$$\dot{Q}_{cv,sg-air} = h_{sg-air} \sum_{i=1}^{n} A_{sw,i} \left(T_{sg} - T_{am}\right)_i \quad (4.4)$$

In the Equation (4.4), $A_{sw}$is the surface area of slit glazed. The temperature of slit glazed introduced by T_{sg}. n is the number of glass panes. The convection heat transfer coefficient between the slit glazed and air (h_{sg-air}) can be determined by

$$h_{sg-air} = Nu_t k_{air}/t \quad (4.5)$$

Conductivity of air is K_{air} and t is the width of slit glazed. Nusselt number can be calculated by

$$Nu_t = 2.75(sw/t)^{-1.2} Re_t^{0.43} + 0.011\phi Re_t (V_{wind}/V_t)^{0.48} \quad (4.6)$$

Where ∅ is the porosity of gap distances and V_t is the velocity of air inside the gap distance region. Reynuld number is calculated by

$$Re_t = (\rho_{air} v_t t)/\mu_{air} \quad (4.7)$$

4.3.1.1 Convective Heat Transfer from Absorber Plate to Plenum Air and Surrounding

The convective heat transfer between the absorber plate and plenum air is related to convection heat transfer ($h_{cv,ap-pla}$), surface area of absorber plate (A_{ap}), and temperature difference between the absorber plate (T_{ap}) and temperature plenum air (T_{pla})

$$\dot{Q}_{cv,ap-pla} = h_{cv,ap-pla} A_{ap} \left(T_{ap} - T_{pla}\right) \quad (4.8)$$

The convection heat transfer coefficient between the absorber plate and plenum air could be determined by the following correlation (Duffie, Beckman, & Worek, 2003).

$$h_{cv,ap-pla} = Nu_{pl} K_{air} / d_{pl} \quad (4.9)$$

d_{pl} is the plenum height and Nu_{pl} can be calculated by

$$Nu_{pl} = 0.664 Re_{pl}^{0.5} Re_{pl}^{0.333} \quad (4.10)$$

$$Re_{pl} = (\rho_{air} v_{pl} d_{pl}) / \mu_{air} \quad (4.11)$$

$$Pr_{pl} = (C_{p,air} \mu_{air}) / K_{air} \quad (4.12)$$

Where v_{pl} is the velocity of air inside the plenum.

The convective heat transfer between the absorber plate and surrounding is determined by

$$\dot{Q}_{cv,ap-sur} = h_{ap,sur} A_{ap} \left(T_{ap} - T_{amb}\right) \quad (4.13)$$

Where the convection heat transfer between the absorber plate and surrounding $h_{ap,sur}$ is calculated by following equations.

$$h_{cv,ap,-sur} = Nu_{ap,sur} K_{air} / W_{ap} \quad (4.14)$$

W_{ap} is the absorber plate width.

$$Nu_{ap,sur} = 0.664 Re_{ap,sur}^{0.5} Re_{ap,sur}^{0.333} \quad (4.15)$$

$$Re_{ap,sur} = (\rho_{air} v_{pl} W_{ap}) / \mu_{air} \quad (4.16)$$

$$Pr_{ap,sur} = (C_{p,air} \mu_{air}) / K_{air} \quad (4.17)$$

The heat loss through the sides is

$$\dot{Q}_{loss} = U_{sp} A_{sp} \left(T_{pla} - T_{amb}\right) \quad (4.18)$$

Where $U_{sp} = 1/\left(1/h_{pl} + R_{sp} + 1/h_{sp,surr}\right)$ is the overall heat transfer coefficient of the side plates of the collector.

4.3.2 Radiation Heat Transfer

The radiation heat transfer is estimated using the Stefan-Boltzman law, which is related to the absolute temperature of the radiating body, surface area and Stefan-Boltzman constant.

4.3.2.1 Radiation Heat Transfer from Slit Glazed to Surrounding

The radiation heat transfer between the slit glazed and surrounding is determined by

$$\dot{Q}_{r,sg-sur} = \varepsilon_{sg} \sigma A_{sg} \left(T_{sg}^4 - T_{gnd}^4 - T_{sky}^4\right) \quad (4.19)$$

Where $\varepsilon_{sg}$is the emissivity of slit glazed. The ground temperature T_{gnd} can be taken as ambient temperature, and the sky temperature is obtained by the following equation

$$T_{sky} = 0.0552T_{amb}^{1.5} \tag{4.20}$$

4.3.2.2 Radiation Heat Transfer between Absorber Plate to Slit Glazed

The radiation heat transfer between the absorber plate and slit glazed is estimated by

$$\dot{Q}_{r,ap-sg} = \sigma A_{ap}\left(T_{ap}^4 - T_{sg}^4\right)/\left(1/\varepsilon_{ap} + 1/\varepsilon_{sg} - 1\right) \tag{4.21}$$

σ is the Stefan–Boltzmann constant.

4.3.2.3 Radiation Heat Transfer from Absorber Plate to Surrounding

The heat loss due radiation from back of absorber plate to surrounding is determined by

$$\dot{Q}_{r,ap-sur} = \varepsilon_{ap}\sigma A_{ap}\left(T_{ap}^4 - T_{gnd}^4 - T_{sky}^4\right) \tag{4.22}$$

The experimental results are presented in the following chapter.

Chapter 5

RESULTS AND DISCUSSIONS

A novel design of SAH with slit glazed cover plate is investigated experimentally. The main aim of this experiment is to improve the thermal performance of the conventional SAH by modifying its design. In this chapter the effect of bed heights of the collector on the thermal performance of the SGSAH is investigated at various gap distances and mass flow rates (series I). Then in series II, the effect of the width of glass panes on the thermal efficiency is experimentally investigated. Finally in series III, the experimental results of the UTC and the SGSAH are compared at mass flow rates less than 0.029 kg/s

5.1 The Effect of Bed Height of the Duct of SGSAH (Series I)

5.1.1 Variation of Solar Intensity and Ambient Temperature with Time

Figure 5.1 shows the mean hourly variation on solar radiation and ambient temperature. The solar intensity increased steadily during the morning hours reaching to a maximum value at midday and then decreased gradually until sunset. The behavior was, by and large, consistent during the entire course of measurements. The ambient temperature increased during the day until afternoon and reduced briefly thereafter. During the experiments, the highest value of solar intensity was measured as 896 W/m^2 with average value of 682 W/m^2 and the maximum ambient temperature (T_{in}) was recorded to be 35°C where the average value was 31°C.

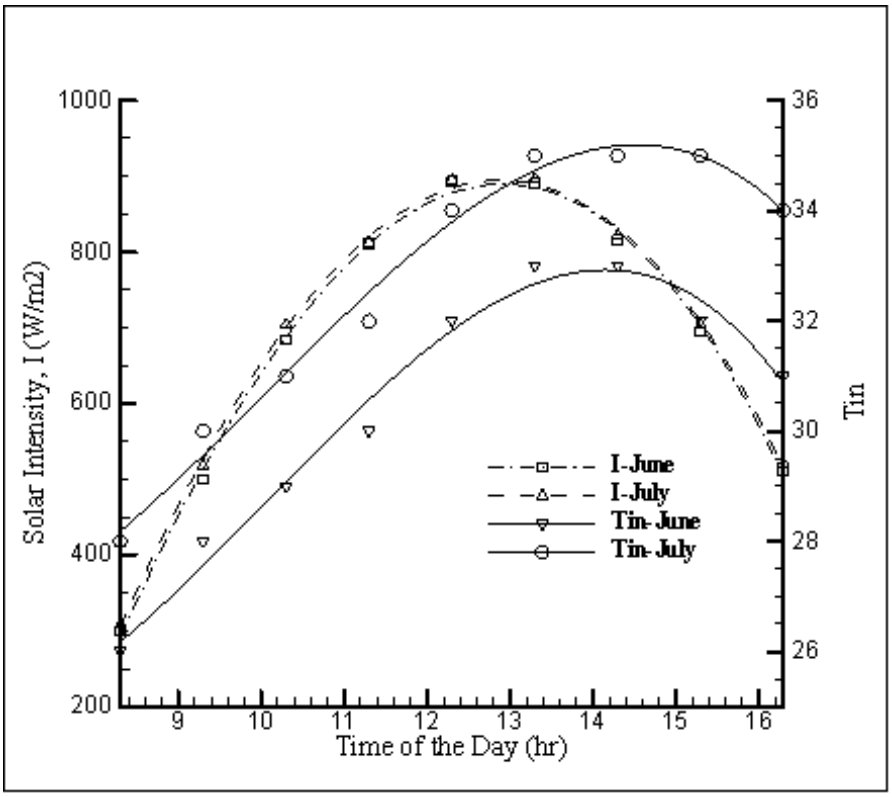

Figure 5. 1:Mean hourly variations of solar intensity and ambient temperature.

5.1.2. The Temperature Rise ΔT (=Tout-Tin) as a Function of Time

The variation of ΔT versus standard local time of the day time for different gap distances, bed heights, and mass flow rates are demonstrated in Figs. 5.2-5.5. ℃

For a gap distance of 0.5 mm (Fig. 5. 2), the ΔT for different mass flow rates increased during the morning hours, reached maximum between 12:30 and 13:30 and then decreased until sunset. The maximum temperature rise was 27°C at the bed height of 7 cm, the least value of mass flow rate of 0.014 kg/s and at 13:30 hr. The lowest value of the maximum ΔT was 12℃ at bed heights of 5 cm and 3 cm, where mass flow rate was 0.057 kg/s at 13:30 hr.

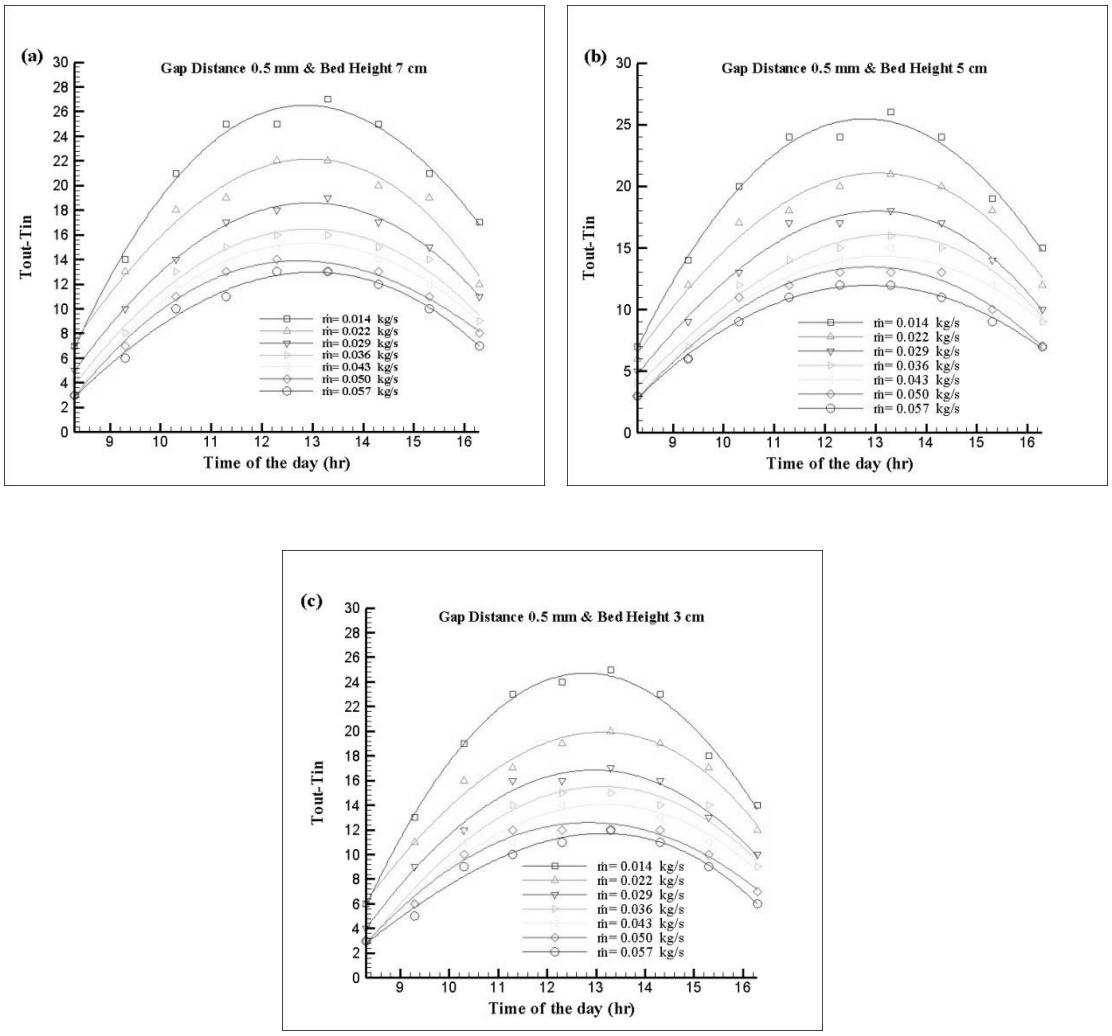

Figure 5. 2:Temperature rise versus time at a gap distance of 0.5 mm for different bed heights: (a) 7 cm, (b) 5 cm and (c) 3 cm.

The results of the maximum temperature rise of the bed height of 3 cm, 5 cm and 7 cm for several mass flow rates are illustrated in Table 5.1.

Table 5. 1:The maximum value of temperature rise: gap distance of 0.5 mm for bed height of 7 cm, 5 cm and 3 cm.

ṁ (kg/s)	0.014	0.022	0.029	0.036	0.043	0.050	0.057
Bed height	Maximum temperature rise, ΔT_{max}						
7 cm	27℃	22℃	19℃	16℃	16℃	14℃	13℃
5 cm	26℃	21℃	18℃	16℃	15℃	13℃	12℃
3 cm	25℃	20℃	17℃	15℃	15℃	12℃	12℃

On increasing the gap distance to 1 mm, the maximum ΔTs were achieved as 24°C, 25°C and 26°C for the bed heights of 3 cm, 5 cm and 7 cm, respectively, for the minimum mass flow rate (see Fig 5.3). The lowest value of the maximum ΔT was 10℃ at the bed height of 3 cm and mass flow rate of 0.057 kg/s. The maximum ΔT at different bed heights and mass flow rates are shown in Table 5. 2.

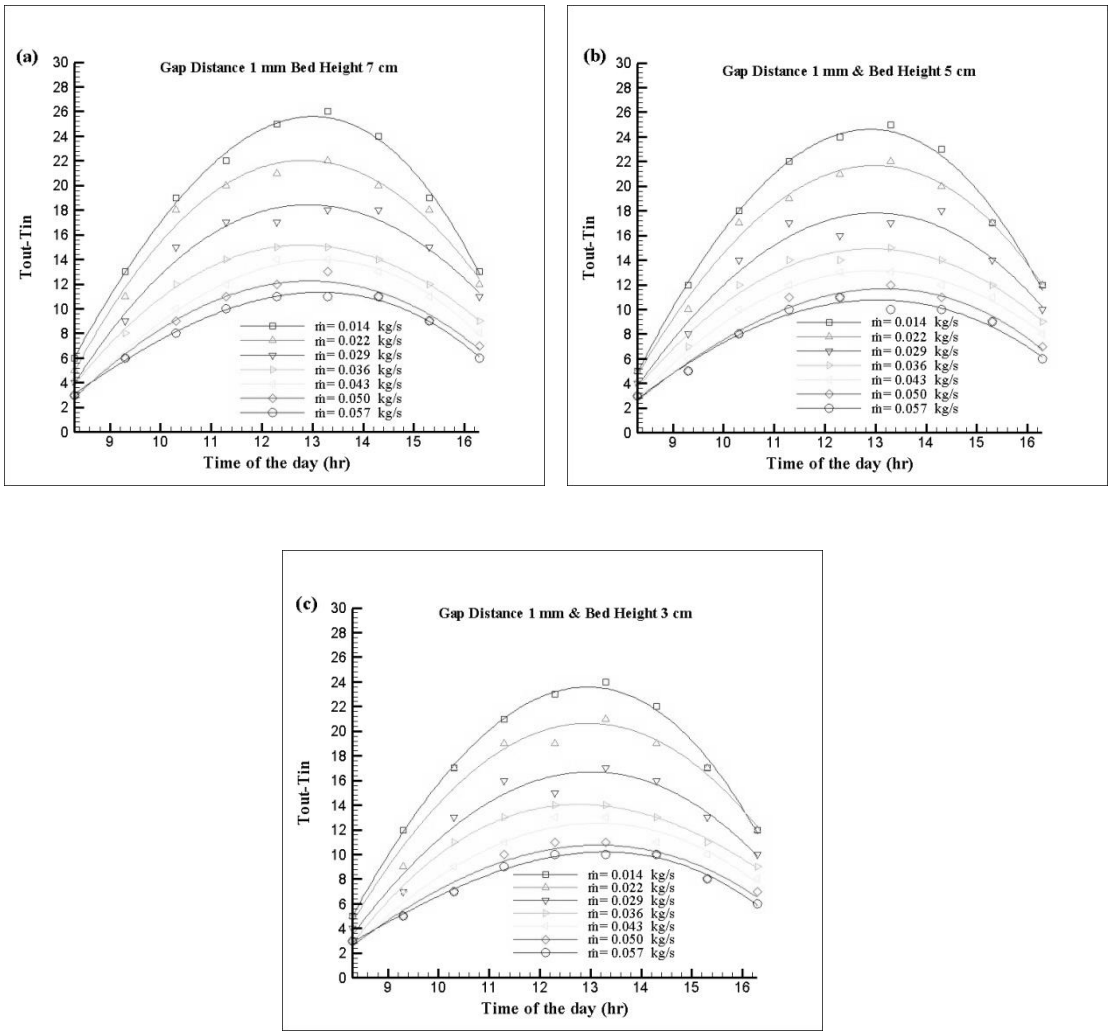

Figure 5. 3:Temperature rise versus time at a gap distance of 1 mm for three different bed heights: (a) 7 cm, (b) 5 cm and (c) 3 cm.

Table 5. 2:The maximum values of temperature rise for gap distance of 1 mm at bed heights of 7 cm, 5 cm and 3 cm.

ṁ(kg/s)	0.014	0.022	0.029	0.036	0.043	0.050	0.057
Bed height	Maximum temperature rise, ΔT_{max}						
7 cm	26℃	22℃	18℃	15℃	14℃	13℃	11℃
5 cm	25℃	22℃	18℃	15℃	13℃	12℃	11℃
3 cm	24℃	21℃	17℃	14℃	13℃	11℃	10℃

However, on increasing the gap distances to 2 mm and 3 mm, the maximum ΔTs were achieved in the SGSAHs where the bed height was 3 cm and mass flow rate was 0.014 kg/s. The ΔT values were low compared to the smaller gap distance values (See Table 5.3 and Table 5.4).

Table 5. 3:The maximum values of temperature rise for gap distance of 2 mm at bed heights of 7 cm, 5 cm and 3 cm.

ṁ(kg/s)	0.014	0.022	0.029	0.036	0.050	0.057
Bed height	Maximum temperature rise, ΔT_{max}					
7 cm	22℃	18℃	15℃	14℃	12℃	11℃
5 cm	23℃	19℃	16℃	13℃	12℃	11℃
3 cm	24℃	20℃	17℃	14℃	11℃	10℃

Table 5. 4:The maximum values of temperature rise for gap distance of 3 mm at bed height of 7 cm, 5 cm, and 3 cm.

ṁ(kg/s)	0.014	0.022	0.029	0.036	0.043	0.050	0.057
Bed height	Maximum temperature rise, ΔT_{max}						
7 cm	21℃	19℃	16℃	14℃	13℃	12℃	10℃
5 cm	21℃	20℃	17℃	14℃	13℃	12℃	10℃
3 cm	22℃	20℃	18℃	15℃	12℃	11℃	9℃

The results (Table (5-4)), indicated that the lowest values of the ΔT_{max} were obtained 10℃ for the gap distance of 2 mm and 9℃ for the gap distance of 3 mm where the bed heights were 3 cm and the mass flow rates were 0.057 kg/s in both tests. The maximum ΔTs for 2 mm gap distance were obtained as 22℃, 23℃ and 24℃ where

the bed heights were 7 cm, 5 cm and 3 cm, respectively, at the mass flow rate of 0.014 kg/s (Fig 5.4). The maximum ΔTs for 3 mm gap distance were obtained as 21℃, 21℃ and 22℃ for the bed heights of 7 cm, 5 cm and 3 cm, respectively, at the lowest mass flow rate of 0.014 kg/s (Fig 5.5).

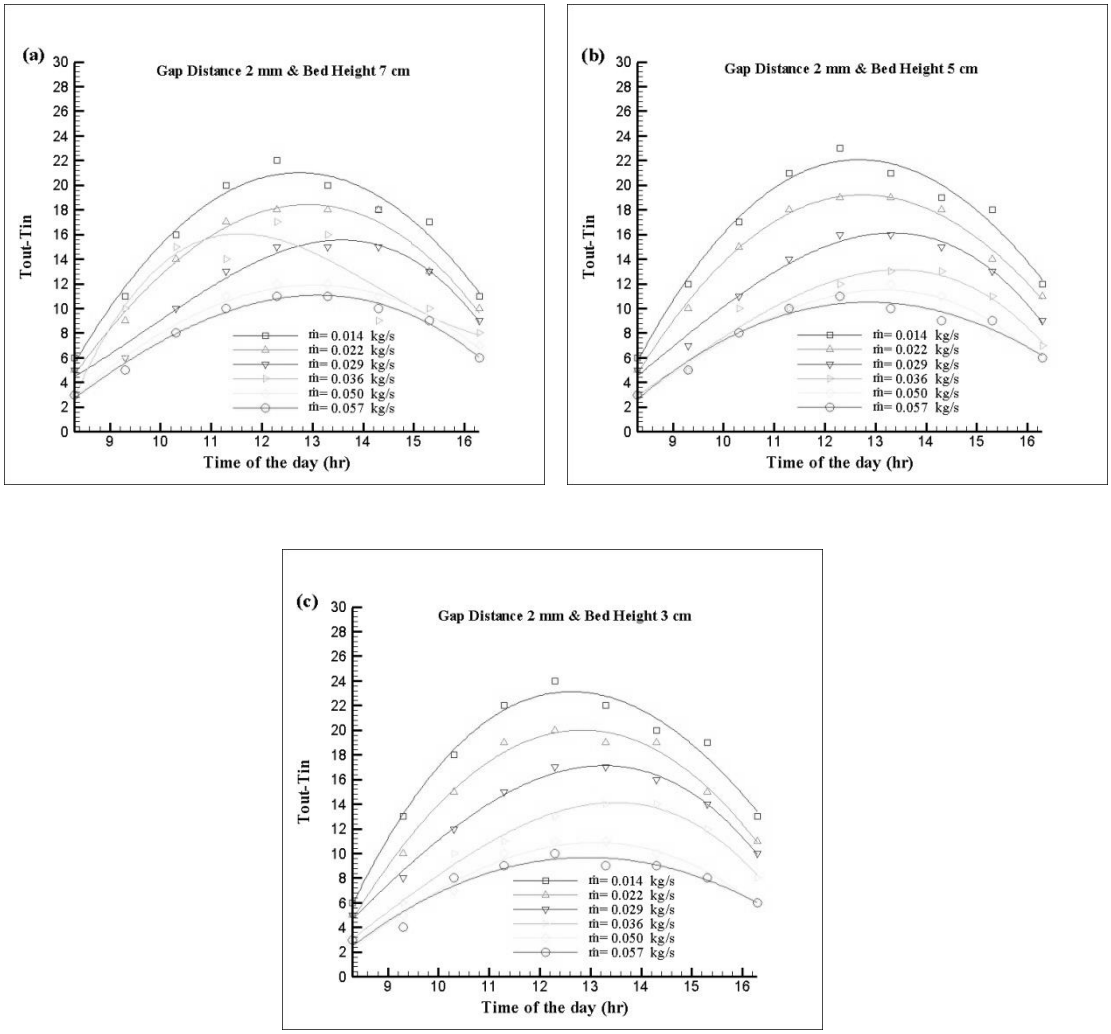

Figure 5. 4:Temperature rise versus time at a gap distance of 2 mm for three different bed heights: (a) 7 cm, (b) 5 cm and (c) 3 cm.

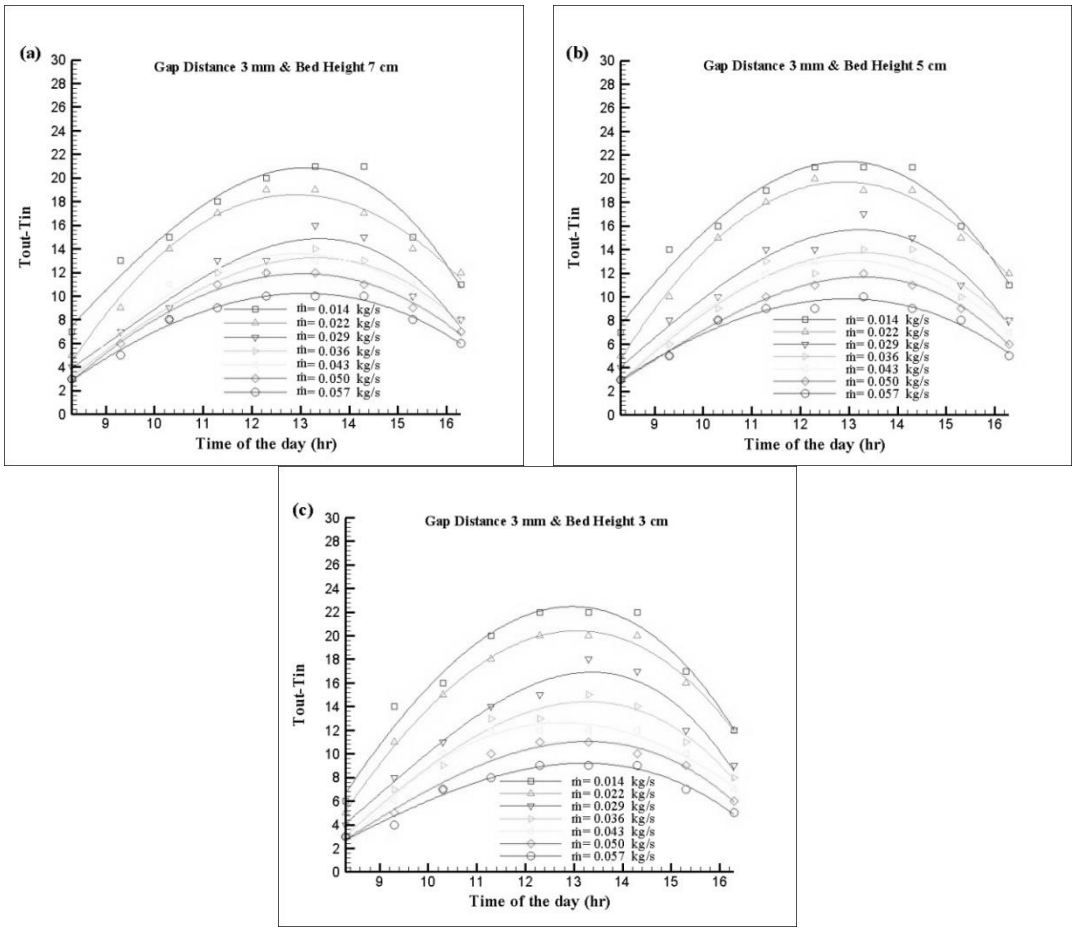

Figure 5. 5:Temperature rise versus time at a gap distance of 3 mm for three different bed heights: (a) 7 cm, (b) 5 cm and (c) 3 cm.

The inlet velocity at smaller gap distance is higher compared with the inlet velocity of bigger gap distance. As friction increases at lower gap distance, the inlet air contact area with glass panes also increased. Therefore, convective and radiation losses decreased at smaller gap distance. Higher inlet velocity increases heat gain due convection from the glass panes. Therefore, it is expected to have higher ΔT at lower gap distance. There is also more possibility for a reversal flow in a higher gap distance SAH leading to lower ΔT.

The experimental findings revealed that:

a) for lower mass flow rates (0.014−0.036) kg/s, (i) for wider gaps (2 mm and 3 mm), higher temperature differences were obtained in the SGSAH with lower bed heights (3 cm) and (ii) for smaller gaps (0.5 mm and 1 mm), higher temperature differences were obtained for higher bed heights, i.e., 7 cm. The highest value of ΔT (27°C) was obtained for the gap distance of 0.5 mm, where the mass flow rate was minimum 0.014 kg/s and bed height was 7 cm. The highest ΔT values (for any bed height) gradually decreased on increasing the gap distances from 0.5 mm to 3 mm. Therefore, for low mass flow rates, the performance of the SGSAH with 3 cm bed height was higher than the other two SGSAHs at wider gaps and the SGSAH with 7 cm bed height performed better than others for smaller gaps.

b) For higher mass flow rates (0.043-0.057) kg/s, the SGSAH with bed height of 7 cm achieved higher temperature differences for all gaps compared with other SGSAHs (Figs 5.2-5.5).

c) Air inlet entering through the gaps between the panes continues to gain heat from the absorber plate by convection inside the plenum. There is a possibility that at low mass flow rates and higher bed heights, the working fluid may not fully come in contact with the lower portion of the absorber plate.

5.1.3 Thermal Efficiency vs. Time

(a). For a gap distance of 0.5 mm, the maximum efficiency was obtained as 82% in the SGSAH with bed height of 7 cm and where the mass flow rate was 0.057 kg/s (Fig 5.6.a). The maximum thermal efficiencies of SGSAHs having bed heights 5 cm and 3 cm were found to be 79% and 75%, respectively (Fig 5.6.b) and Fig 5.6.c). In addition, the average efficiencies for the SGSAHs with bed heights of 7 cm, 5 cm,

and 3 cm were found to be 62%, 59%, and 56%, respectively. Hence, the highest values of thermal efficiencies for SGSAH with 0.5 mm gap distance were found where the bed height was 7 cm for all mass flow rates. The average values of thermal efficiencies of bed heights at various mass flow rates are shown in Table 5.5. Results indicated that thermal efficiency increases with increasing mass flow rate at any bed height.

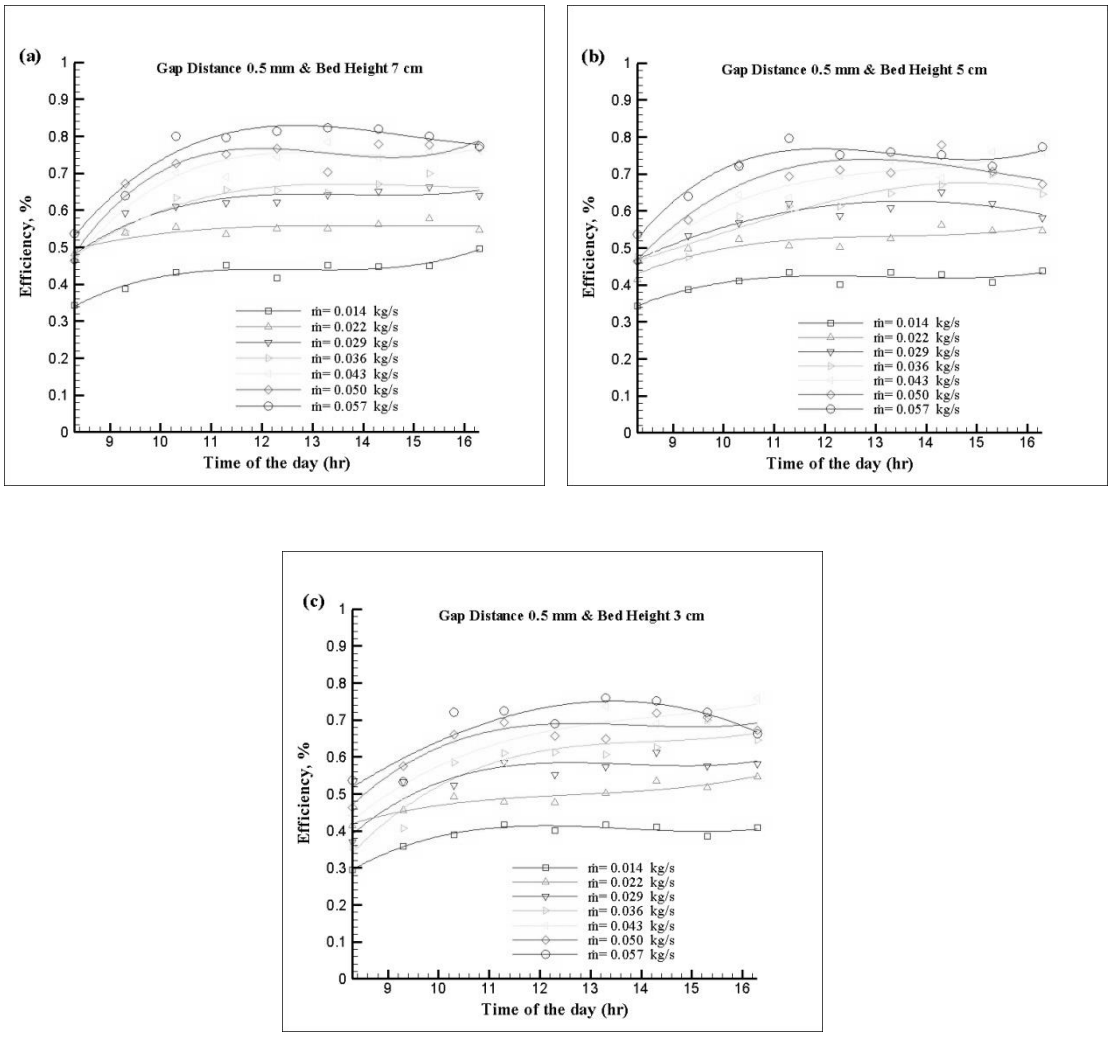

Figure 5. 6:Thermal efficiency versus time at the gap distance of 0.5 mm for bed heights: (a) 7 cm, (b) 5 cm, and (c) 3 cm.

Table 5. 5:The average values of thermal efficiency for gap distance 0.5 mm at bed height of 7 cm, 5 cm and 3 cm.

ṁ (kg/s)	0.014	0.022	0.029	0.036	0.043	0.050	0.057
Bed height	Thermal efficiency, %						
7 cm	43	54	61	62	70	71	75
5 cm	41	51	58	60	66	67	72
3 cm	39	49	54	57	64	64	68

(b). By increasing the gap distance to 1 mm, the maximum thermal efficiency was achieved for the SGSAH with bed height 7 cm as 77% with the mass flow rate as 0.057 kg/s (Fig 5.7.a). The average efficiencies for different bed heights, 7 cm, 5 cm and 3 cm, were 57%, 55%, and 52% respectively (Fig 5.7). This showed an overall decrease in the maximum thermal efficiency obtained for the gap distance of 0.5 mm from 82% to 77%. In addition, the average values of the thermal efficiency of SGSAHs are illustrated in Table 5.6.

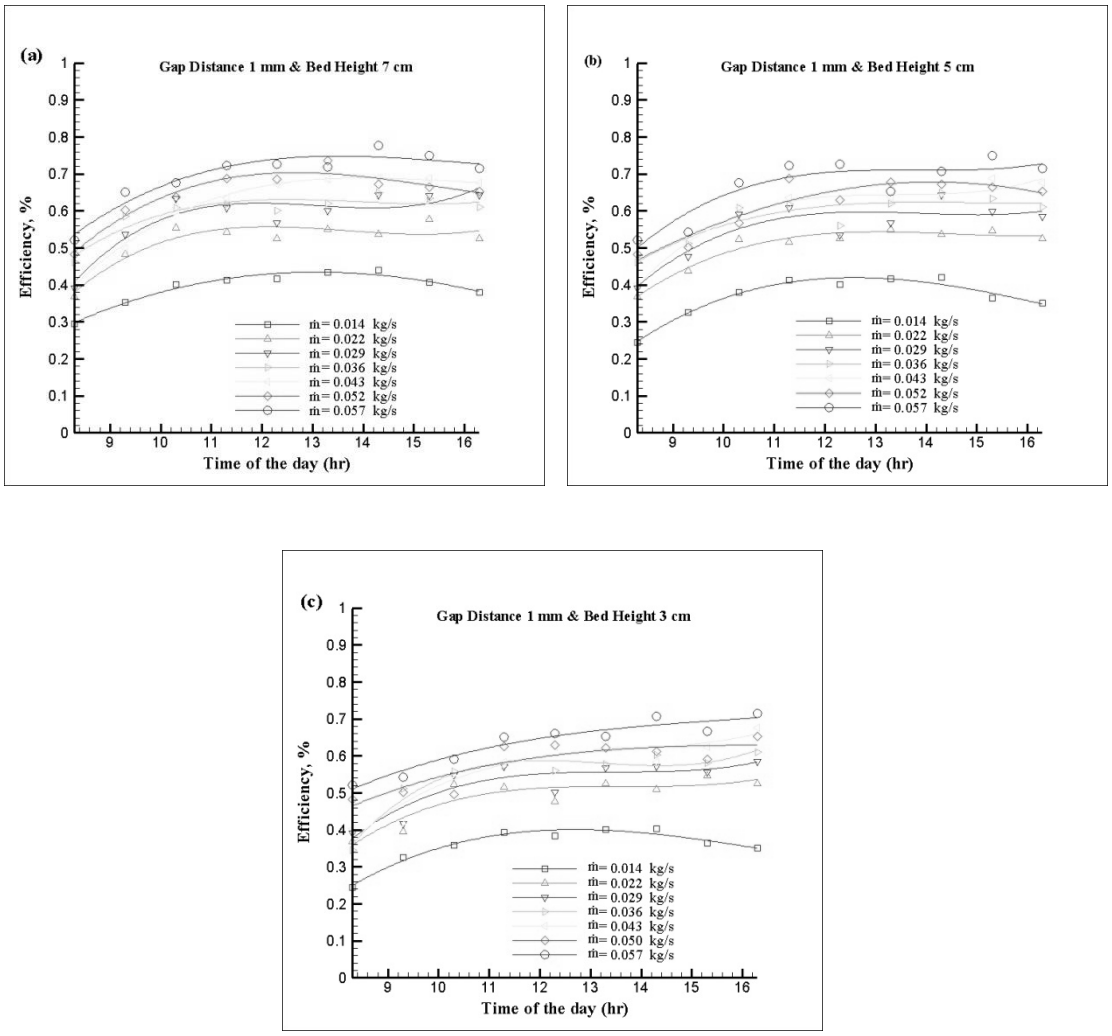

Figure 5. 7:The average values of thermal efficiency for gap distance 1 mm at bed height of 7 cm, 5 cm and 3 cm.

Table 5. 6:The average values of thermal efficiency for gap distance 1 mm at bed height of 7 cm, 5 cm and 3 cm.

ṁ (Kg/s)	0.014	0.022	0.029	0.036	0.043	0.050	0.057
Bed height	Thermal efficiency, %						
7 cm	39	52	58	60	62	65	70
5 cm	37	50	55	59	60	62	67
3 cm	36	49	52	55	57	58	63

(c). As the gap distance was increased to 2 mm, the maximum thermal efficiency was achieved as 75% with bed height 7 cm and maximum mass flow rate, 0.057 kg/s (Fig 5.8.a). For all other mass flow rates with bed height 7 cm, no maximum efficiency was found. The average thermal efficiencies were found to be 50%, 49%, and 49% for bed heights of 7 cm, 5 cm, and 3 cm, respectively. The results also show that, for lower mass flow rates (0.014−0.036) kg/s, the thermal performance of the SGSAH with 3 cm bed height was higher than the other two SGSAHs (Fig 5.8). The maximum efficiency further reduced as the gap distance increased, from 77% in 1 mm case to 75% here.

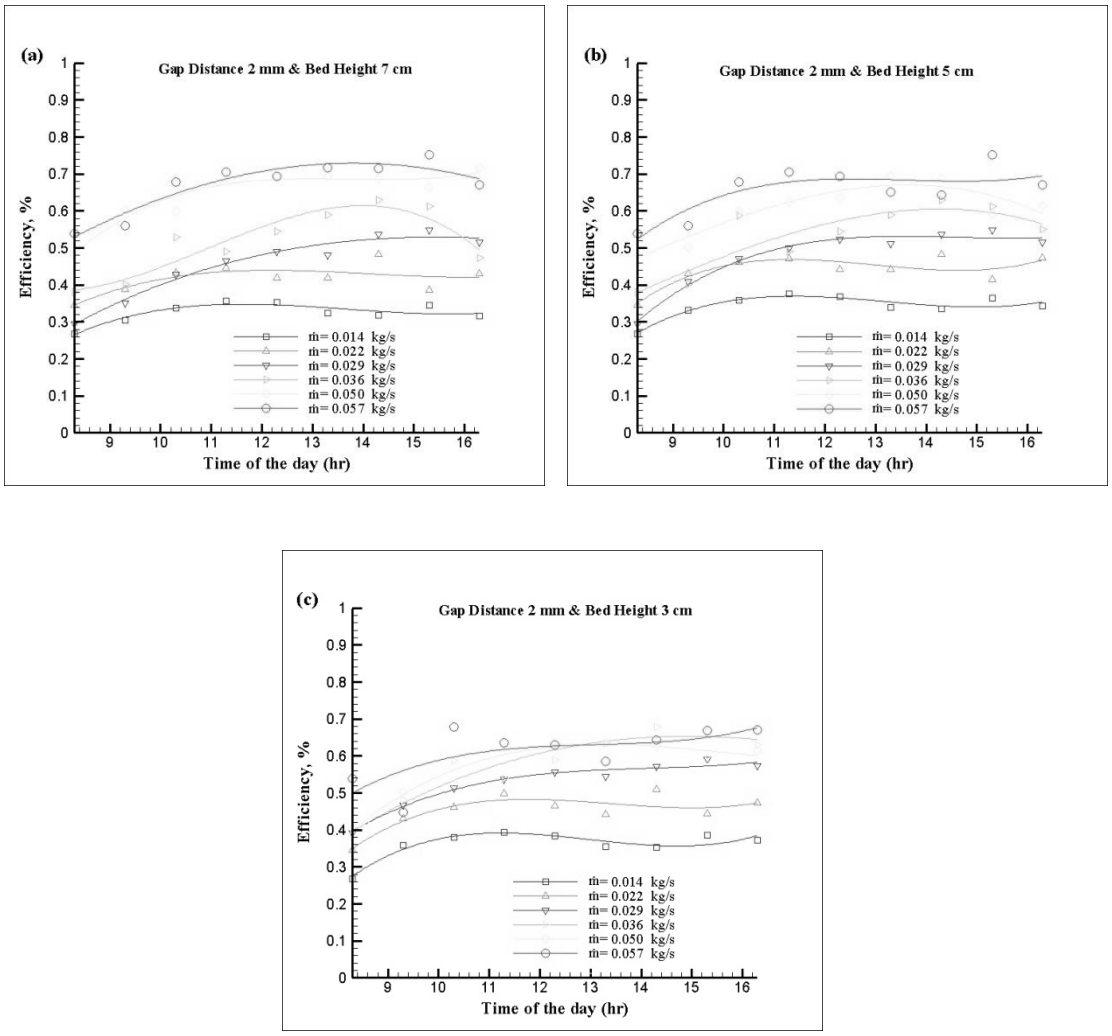

Figure 5. 8:Thermal efficiency versus time at the gap distance of 2 mm for bed heights: (a) 7 cm, (b) 5 cm, and (c) 3 cm.

From Table 5.7, the lowest values of the minimum thermal efficiency were achieved for each bed height at mass flow rate of 0.014 kg/s. In addition, results indicated that the rate of decreasing thermal efficiency by increasing gap distances is significant at lower mass flow rates.

Table 5. 7:The average values of thermal efficiency for gap distance 2 mm at bed height of 7 cm, 5 cm and 3 cm.

ṁ (kg/s)	0.014	0.022	0.029	0.036	0.050	0.057
Bed height	Thermal efficiency, %					
7 cm	32	42	46	55	65	67
5 cm	34	44	48	53	60	65
3 cm	36	45	53	58	57	61

(d). For 3 mm gap distance, the maximum thermal efficiency decreased further (compared to smaller gap distances) to 73% in the SGSAH with bed height 7 cm and the mass flow rate as 0.057 kg/s, Fig 5.9.a). The average thermal efficiencies were obtained as 50% for each of the SGSAH.

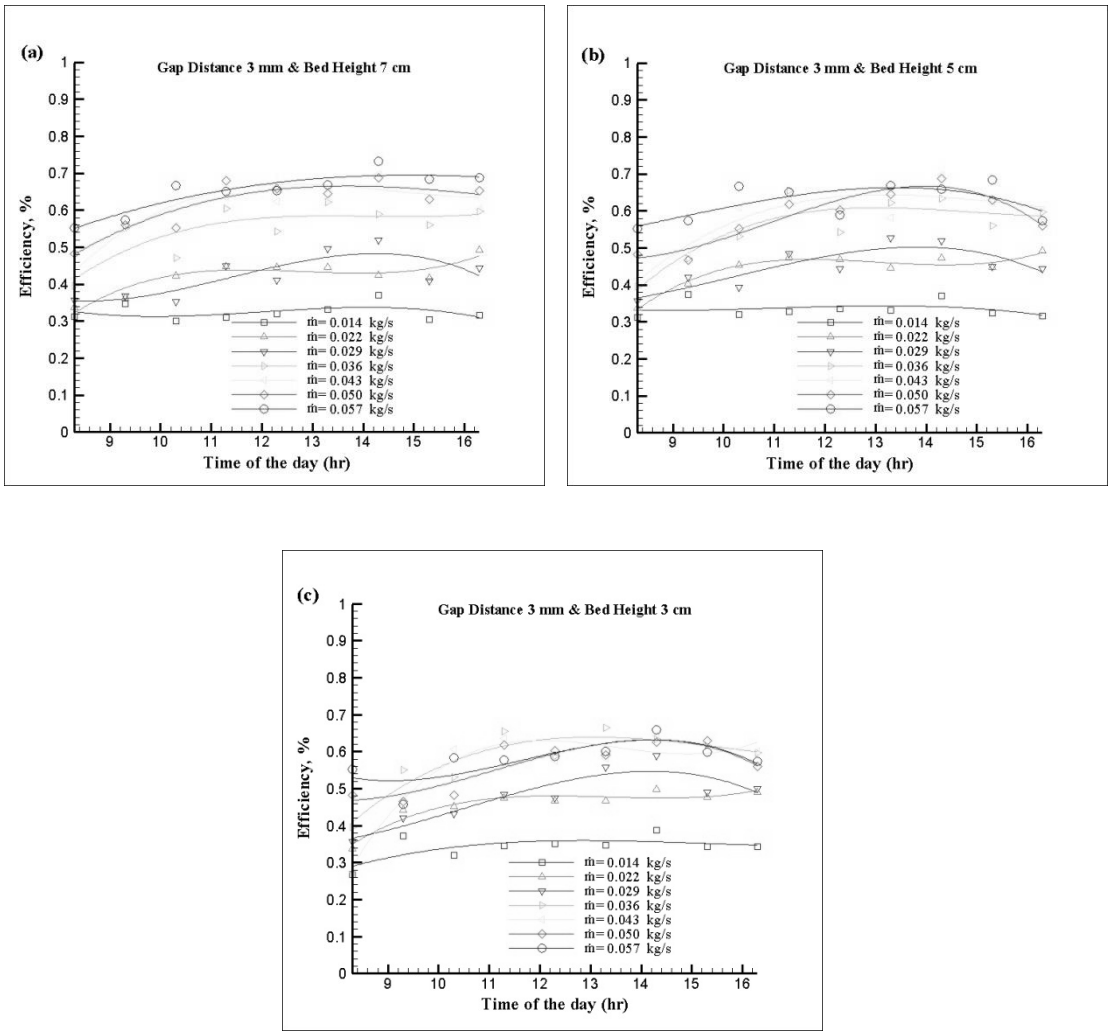

Figure 5. 9:Thermal efficiency versus time at the gap distance of 3 mm for bed heights: (a) 7 cm, (b) 5 cm, and (c) 3 cm.

Table 5.8 shows that the lowest values of maximum thermal efficiency were achieved at the lowest mass flow rate for each bed height as is expected from the previous discussions.

Table 5. 8:The average values of thermal efficiency for gap distance 3 mm at bed height of 7 cm, 5 cm and 3 cm.

ṁ (kg/s)	0.014	0.022	0.029	0.036	0.043	0.050	0.057
Bed height	Thermal efficiency, %						
7 cm	32	42	42	55	61	62	65
5 cm	33	44	45	56	59	58	62
3 cm	34	46	48	56	56	56	58

(e). It is found that the thermal efficiency is significantly dependent on the ambient temperature and it enhances with increasing ambient temperature. At the morning time when the ambient temperature is low, the amount of heat losses is higher from the collectors to the environment compared to the afternoon.

(IV). Efficiency versus $(T_{air}-T_{amb})/I$*:* Figure 5.10. (a)-(c) shows the efficiency versus $(T_{air}-T_{amb})/I$ plot with different mass flow rates for three different bed heights and for a gap distance of 0.5 mm. The thermal efficiency of the SGSAHs increased as $(T_{air}-T_{amb})/I$ ratio increased, steeply for higher mass flow rates than for lower mass flow rates. Also, the thermal efficiencies increased with increasing mass flow rates, as expected. Similar results were obtained in earlier studies(Karmare & Tikekar, 2009; Nowzari, Aldabbagh, & Egelioglu, 2014; Vaziri et al., 2015). The maximum efficiency was obtained for the bed height of 7 cm with maximum mass flow rate. The observations were made for different gap distances which showed a similar pattern. Here, the results related to the most efficient gap distance, 0.5 mm, are presented.

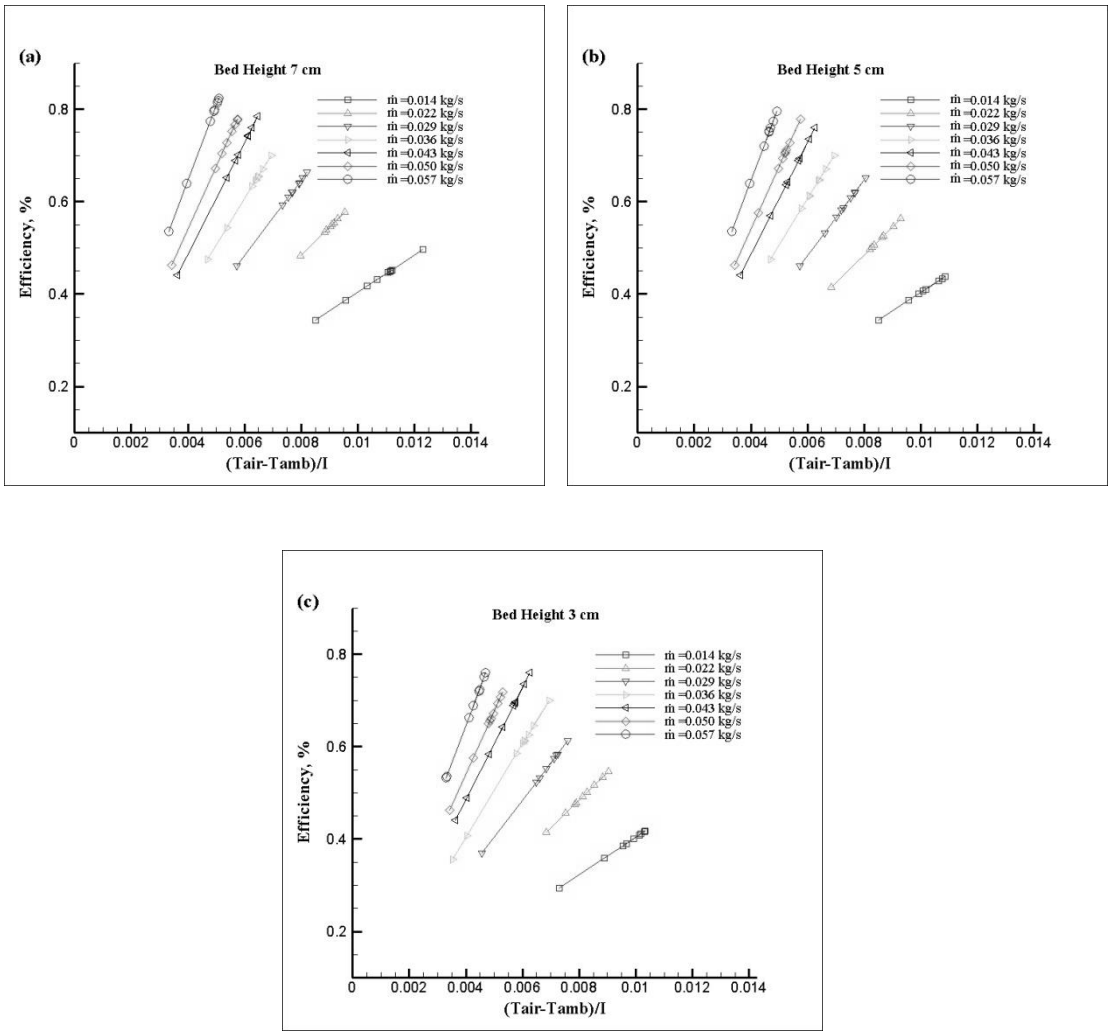

Figure 5. 10:Efficiency versus (Tair-Tamb)/I at a gap distance of 0.5 mm and different mass flow rates for SGSAHs with varying bed heights: (a) 7 cm, (b) 5 cm and (c) 3 cm.

5.2. The Effect of the Width of the Glass Pane (Series II)

5.2.1 Hourly variation of solar intensity and inlet temperature

The variations in solar intensity and the inlet temperature were measured on all working days. Since the results indicated a minor fluctuation in the corresponding curves for different days, a mean value for all the working days was considered. Figure 5.11 illustrates the variations in ambient temperature and solar radiation vs. time.

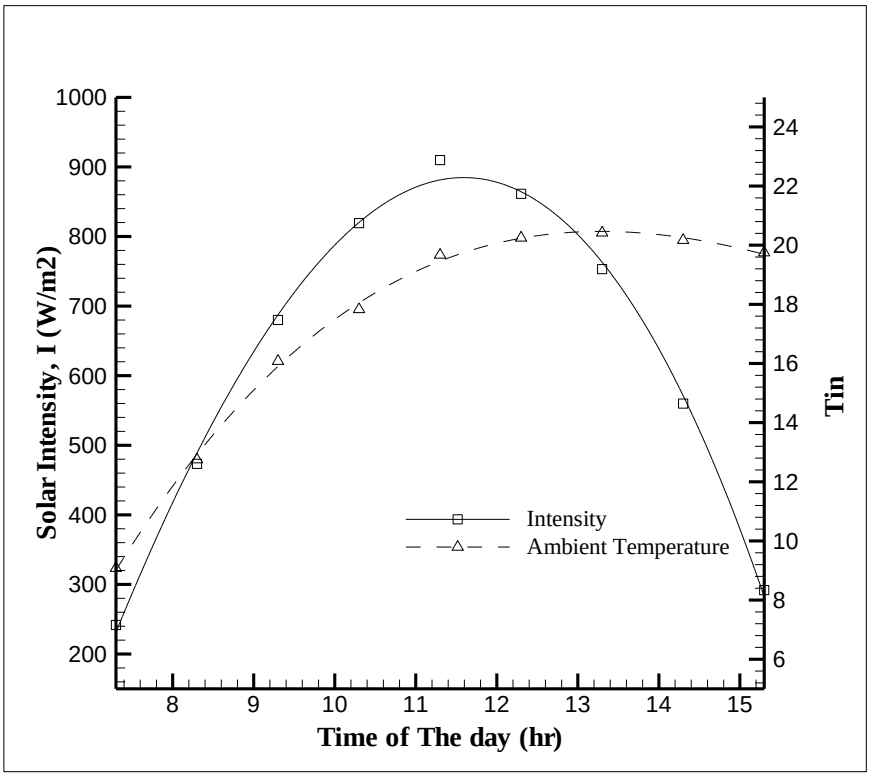

Figure 5. 11:Hourly variations of solar intensity and inlet temperature.

Typically, the solar intensity increased steadily in the morning hours, peaked at midday and reduced thereafter. The maximum solar radiation intensity was noted at 11:30 AM as 923.83 W/m^2 and the mean value was 621.16 W/m^2.

5.2.2 Temperature Rise in the SGSAH

It is known, in general, that the ambient temperature rises during the day till afternoon. The maximum inlet temperature was measured as 23℃ at 01:30 PM. The rise in the temperature for the gap distance of 0.5 mm is illustrated in Fig 5.12 for different slit widths and mass flow rates.

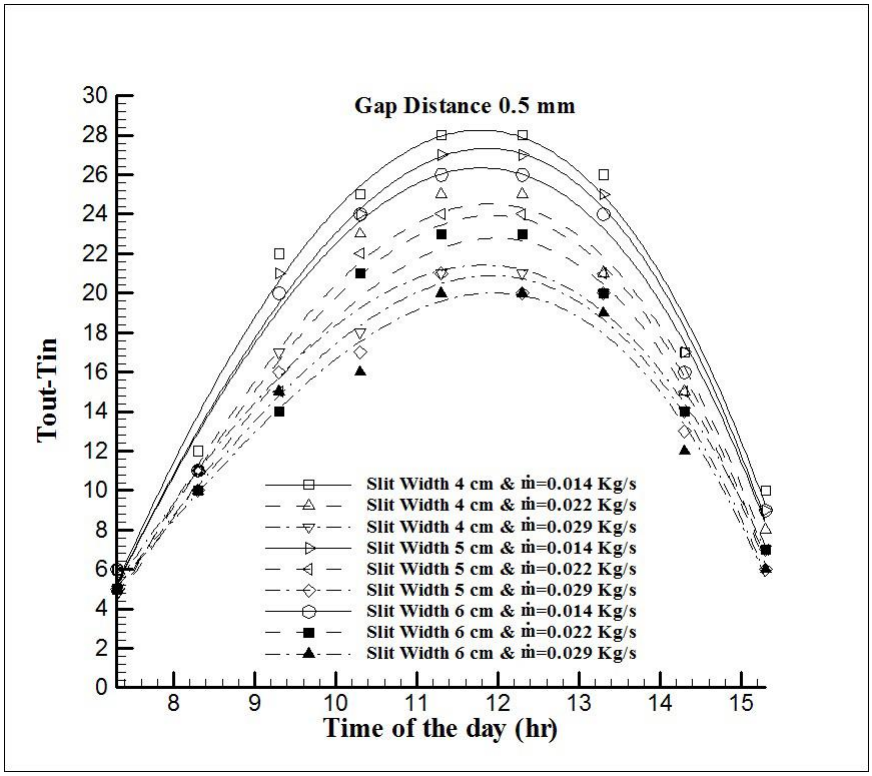

Figure 5. 12:Temperature rise versus time for a gap distance of 0.5 mm and slit widths: 6 cm, 5 cm and 4 cm.

Figure 5.12 shows that for a gap distance of 0.5 mm, the maximum ΔT is 28℃ with the smallest slit width of 4 cm and the lowest mass flow rate of 0.014 kg/s. Similarly, Figure 5.13 shows that for a gap distance of 1 mm, the maximum ΔT is 26℃ for a slit width of 4 cm for the lowest mass flow rate. It also follows from the figures that ΔT rises during morning hours, becomes maximum at midday and then reduces in the afternoon.

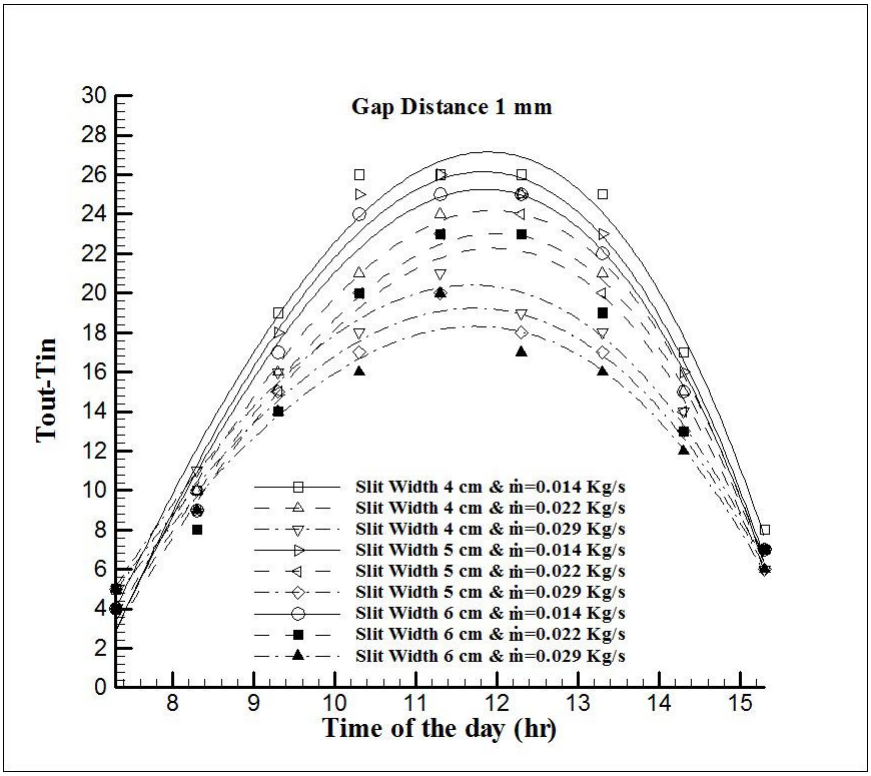

Figure 5. 13:Plot of temperature rise versus time for a gap distance of 1 mm and slit widths: 6 cm, 5 cm and 4 cm.

By increasing the gap distance to 2 mm (Fig 5.14) ΔT decreased for all the values of slit width. The maximum temperature rise is obtained as 23℃ for slit width 4 cm at a lowest mass flow rate of 0.014 kg/s. Clearly, the highest ΔT in all the cases is obtained for the lowest air mass flow rate of 0.014 kg/s.

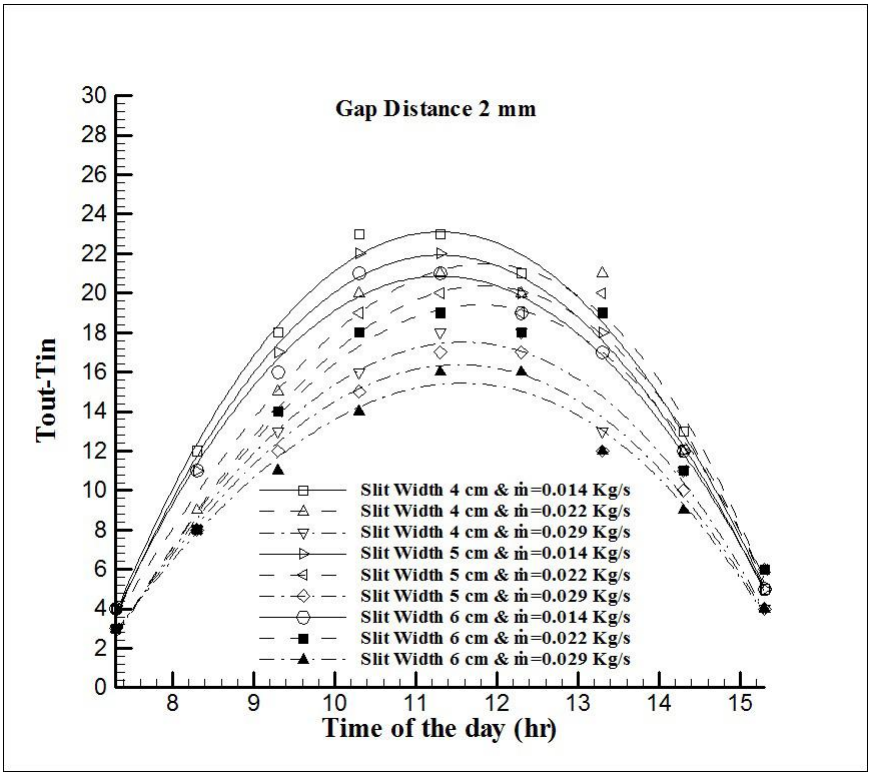

Figure 5. 14:Temperature rise versus time for a gap distance of 2 mm and slit widths: 6 cm, 5 cm and 4 cm.

In the last case as well, for a gap distance of 3 mm (Fig 5.15), the maximum ΔT is obtained as 23℃ with a slit width of 4 cm for the lowest mass flow rate. In general, T_{out} - T_{in} reduces with the increasing mass flow rate.

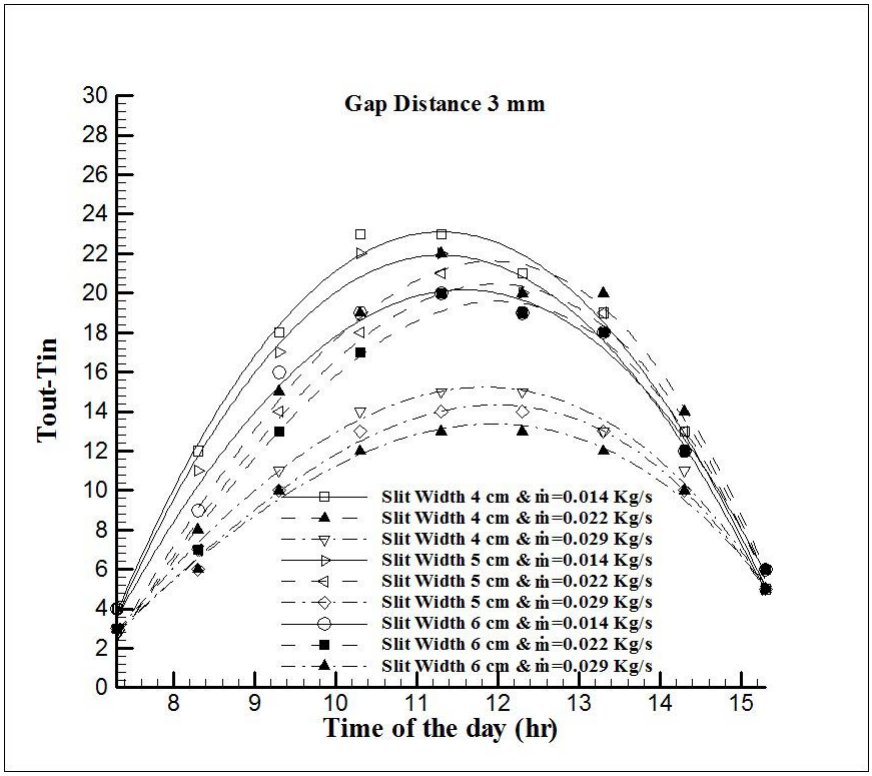

Figure 5. 15:Temperature rise versus time at gap distance of 3 mm and slit widths: 6 cm, 5 cm and 4 cm.

5.2.3 Variation of Thermal Efficiency of SGSAH

The thermal efficiency of SGSAH was investigated for the different gap distances, slit widths, and air mass flow rates. For 0.5 mm gap distance, the maximum efficiency was obtained as 75% for slit width and air mass flow rate of 4 cm and 0.029 kg/s respectively. The highest thermal efficiency, for slit widths 5 cm and 6 cm, were 75% and 71%, respectively (Fig 5.16). The average efficiency values for SGSAHs with 4 cm, 5 cm, and 6 cm slit widths were 57%, 54%, and 52% respectively.

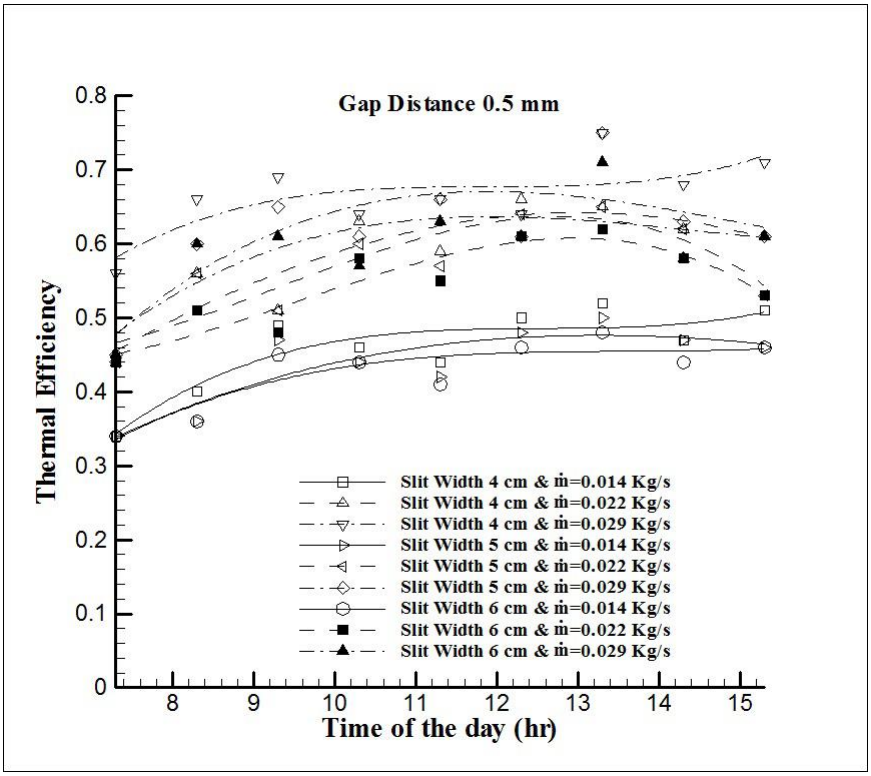

Figure 5. 16:Thermal efficiency versus time for a gap distance of 0.5 mm and slit widths of 6 cm, 5 cm and 4 cm.

For 1-mm gap distance, the highest thermal efficiency was obtained as 70%, 65%, and 65%, when slit widths were 4 cm, 5 cm, and 6 cm, respectively (Fig 5.17). It should be noted that highest thermal efficiency for each slit width occurred when the mass flow rate was maximum, i.e., 0.029 kg/s. The mean values of thermal efficiency were 53%, 50%, and 48%, respectively, at the slit widths of 4 cm, 5 cm, and 6 cm.

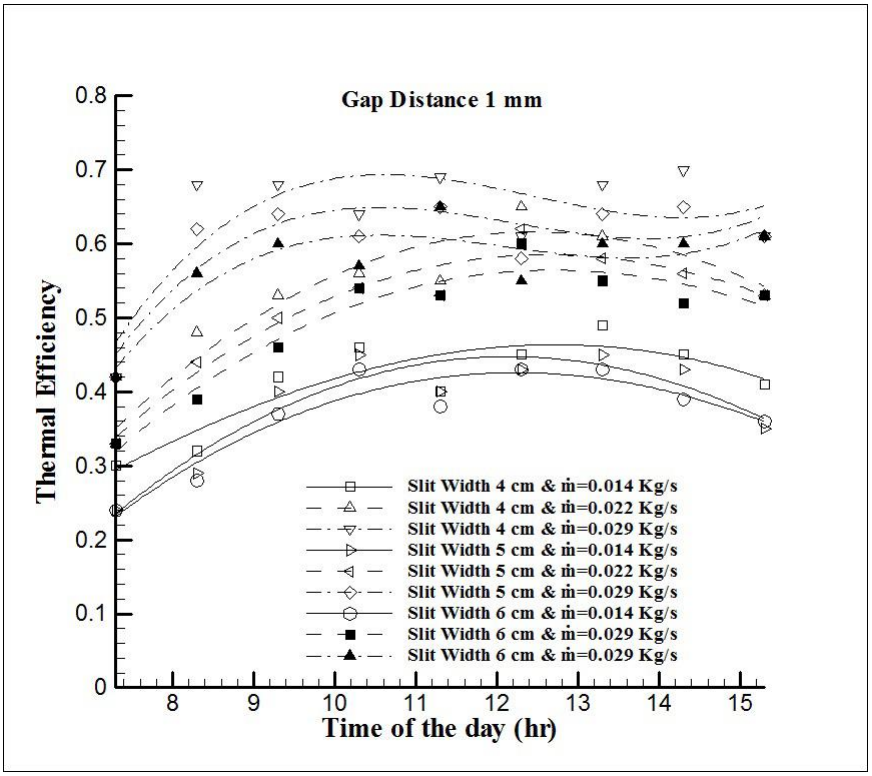

Figure 5. 17:Thermal efficiency versus time for a gap distance of 1 mm and slit widths of 6 cm, 5 cm, and 4 cm.

By increasing the gap distance from 1 mm to 2 mm, the thermal efficiency increased for each slit width. The maximum thermal efficiencies were achieved as 60%, 57%, and 53%, respectively, for slit widths 4 mm, 5 mm, and 6 mm at a maximum air mass flow rate (Fig 5.18). The results demonstrated that the average values of thermal efficiency for all mass flow rates were 44%, 42%, and 40% at the slit widths of 4 cm, 5 cm, and 6 cm, respectively.

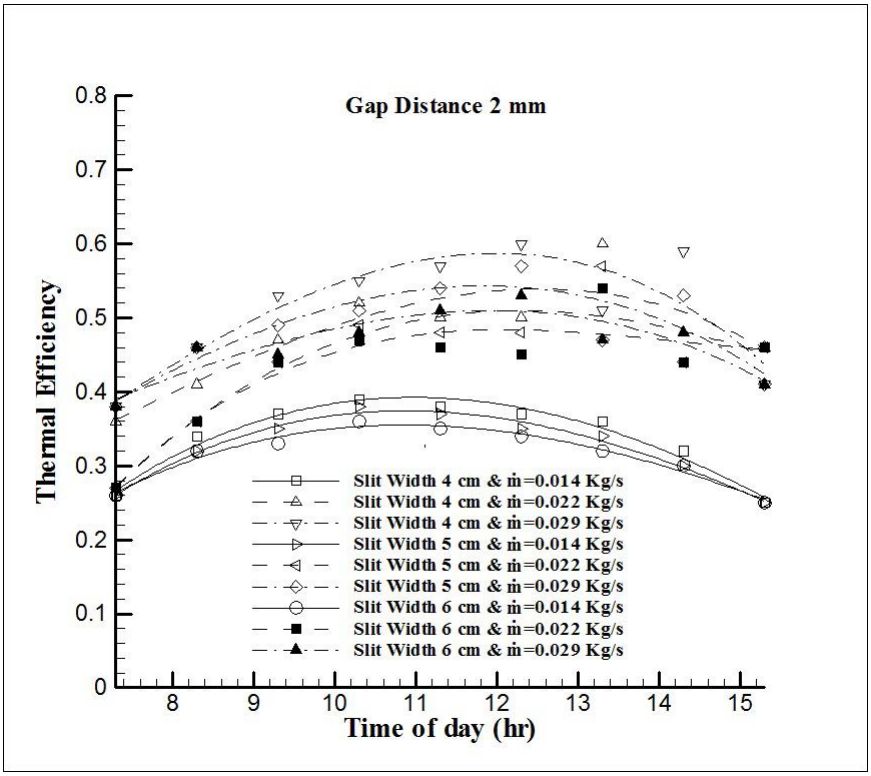

Figure 5. 18:Thermal efficiency versus time at a gap distance of 2 mm and slit widths: 6 cm, 5 cm and 4 cm.

On increasing the gap distance from 2 mm to 3 mm, the thermal efficiency is decreased. The maximum thermal efficiency at 4 cm slit width was found to be 56%. The maximum thermal efficiencies were calculated to be 51% for both 5 cm and 6 cm glass slits (Fig 5.19). The average values of efficiency for the slit widths of 4 cm, 5 cm, and 6 cm were obtained as 42%, 40%, and 38%, respectively.

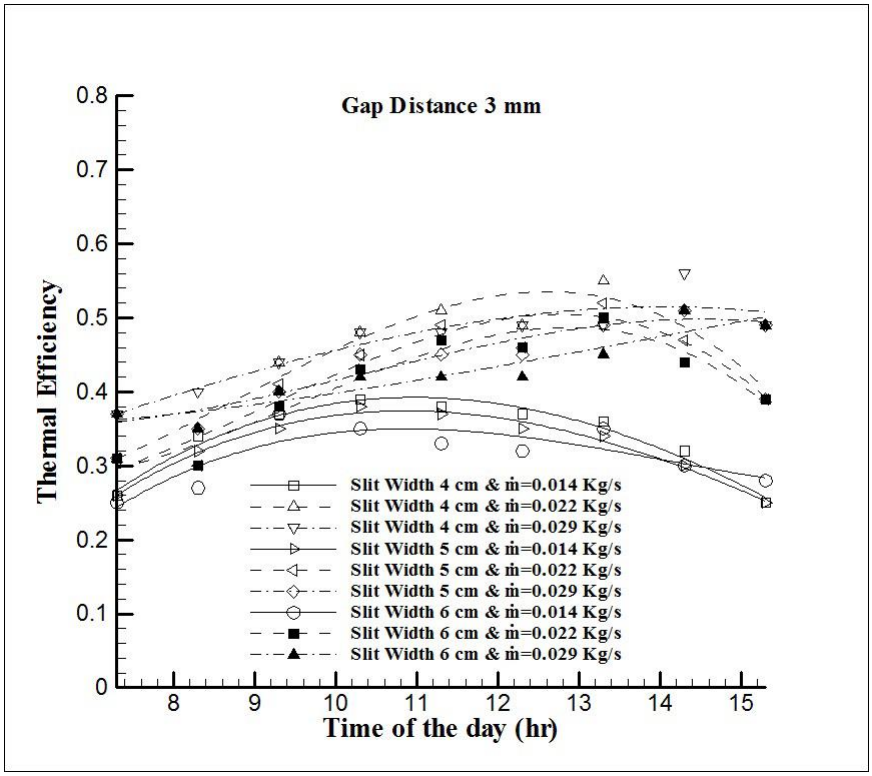

Figure 5. 19:Thermal efficiency versus time for a gap distance of 3 mm and slit widths of 6 cm, 5 cm and 4 cm.

The variation of $(T_{air}-T_{amb})/I$ versus thermal efficiency are presented in Fig. 5.20. The results demonstrated that thermal efficiency and slope of the thermal efficiency versus $(T_{air}-T_{amb})/I$ increased by increasing mass flow rates. The highest efficiency was obtained where the gap distance was 0.5mm. In this study the variation of $(T_{air}-T_{amb})/I$ versus thermal efficiency of SGSAHs with 0.5 mm gap distances are presented.

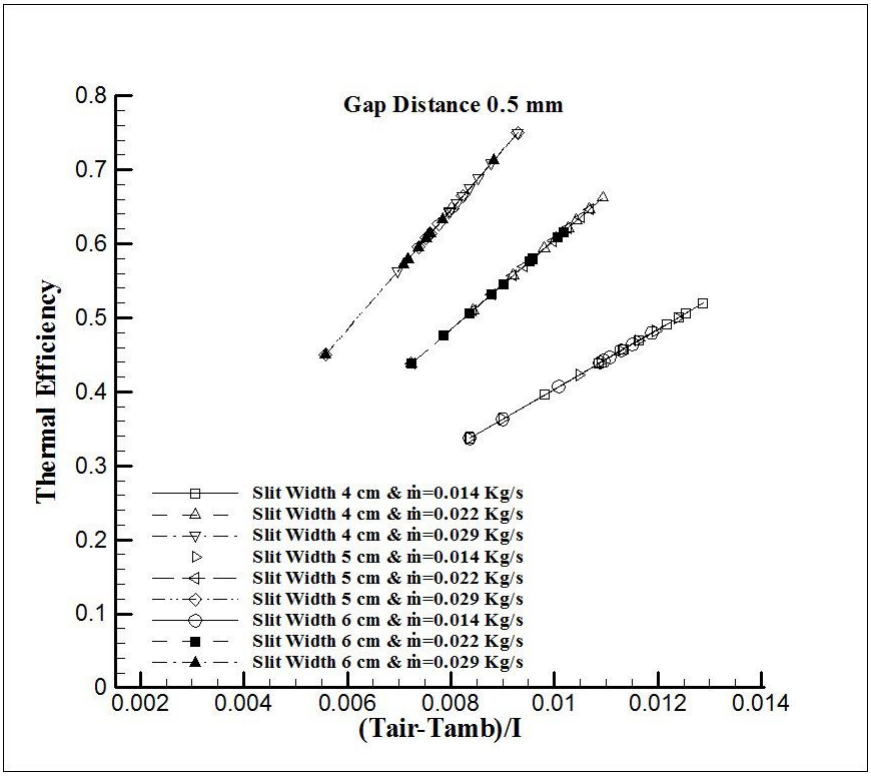

Figure 5. 20:Thermal efficiency versus Tair-Tamb /I at gap distance of 0.50 mm and slit widths of 6 cm, 5 cm and 4 cm.

5.3 Comparison between the SGSAH and UTC (Series III)

5.3.1 Hourly Variation of Solar Intensity and Ambient Temperature

During the series III experiments, the variation of solar intensity and inlet temperature versus time is illustrated in Fig. 5.21. The maximum intensity and ambient temperature was 850 W/m^2 and 20℃, respectively. The average value of solar irradiation was noted 589 W/m^2

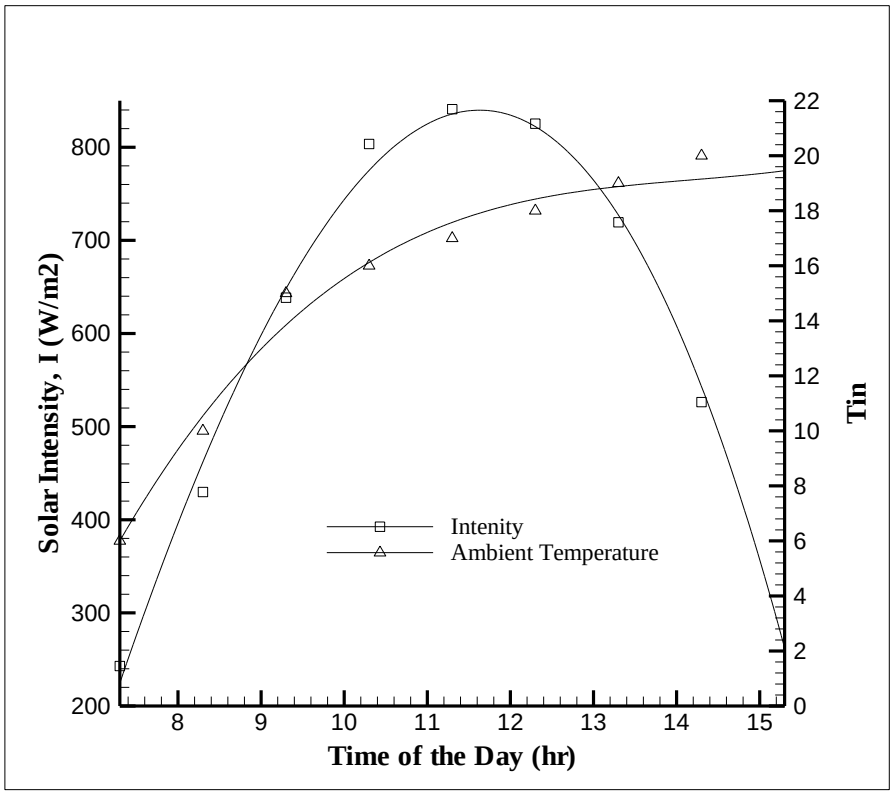

Figure 5. 21:The hourly variation of solar intensity and ambient temperature.

5.3.2 Temperature raise and Thermal Efficiency of SGSAH and UTC

The experimental results of a SGSAH with gap distance of 3 mm, bed height of 7 cm and slit width of 4 cm are compared with a UTC in Figs 5.22-5.23. The experimental results indicated that the maximum ΔT was 17℃ and 11℃, respectively for SGSAH and UTC, at the lowest mass flow rate (0.014 kg/s).

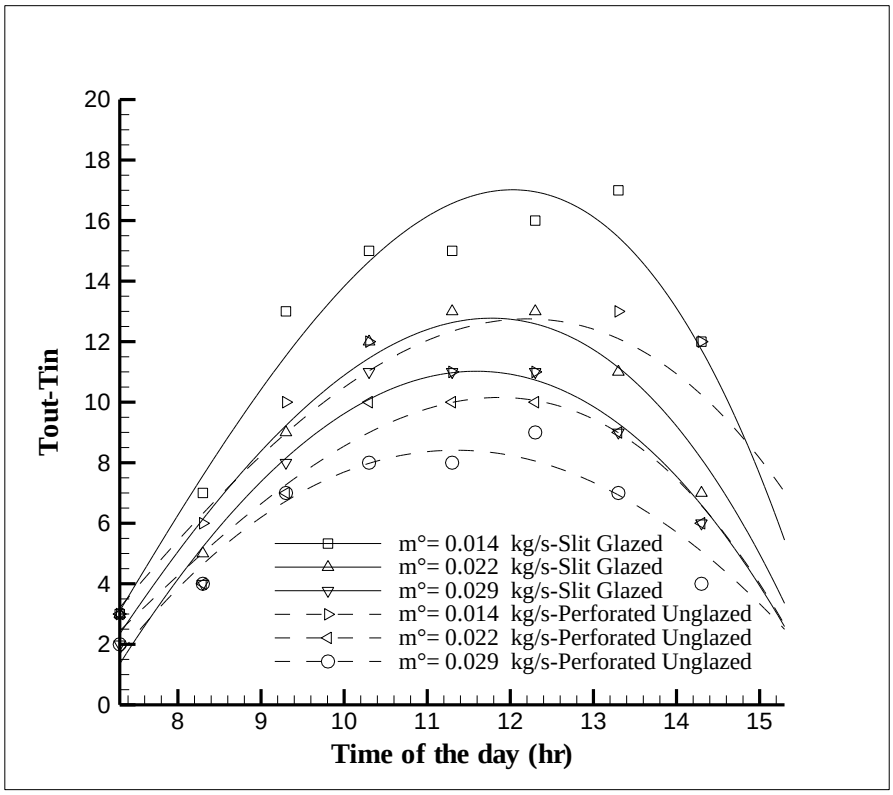

Figure 5. 22:Temperature rise versus time of SGSAH and UTC for mass flow rates of (0.014, 0.022, and 0.029) kg/s.

The experimental results show that the maximum thermal efficiency of SGSAH and UTC was 54% and 46%, respectively, which was noted at the highest mass flow rate of 0.029 kg/s.

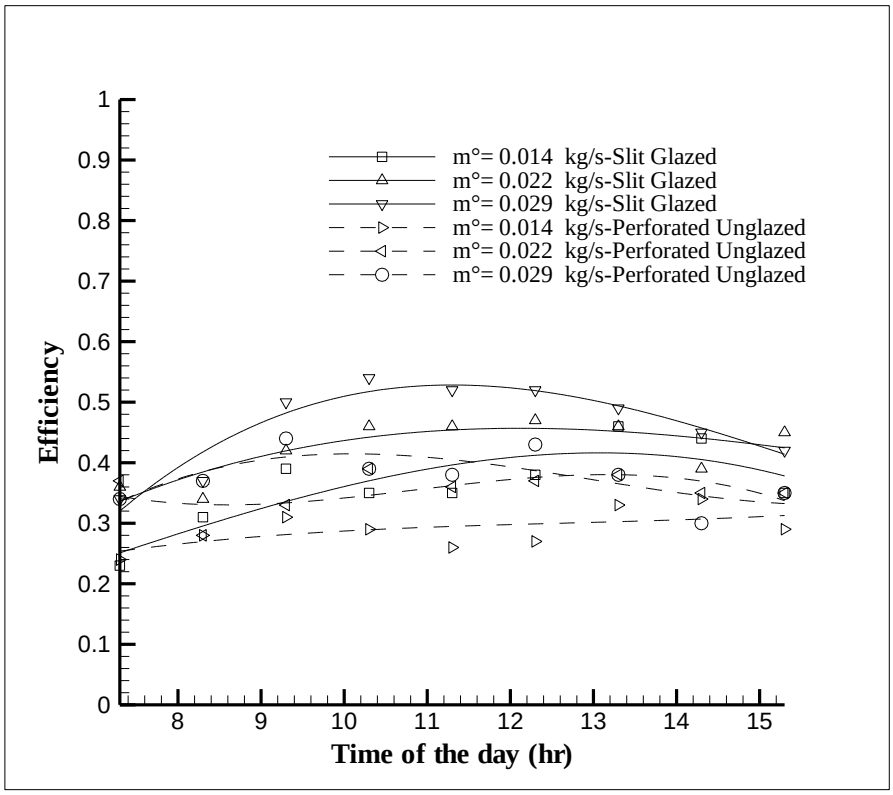

Figure 5. 23:Thermal efficiency versus time of SGSAH and UTC for mass flow rates of (0.014, 0.022, and 0.029) kg/s.

Chapter 6

CONCLUSION

6.1 The Effect of Bed Height of the Duct (Series I)

The performances of three different SGSAHs at various gap distances, mass flow rates, slit width and for different bed heights were investigated experimentally in terms of the following observables: (i) solar intensity and ambient temperature, (ii) temperature rise of the outlet air and (iii) thermal efficiency. A new design for SAHs was proposed in this study to minimize the glazing heat losses that are present in a conventional SAH.

The results indicated that by increasing mass flow rate, ΔT decreased while the thermal efficiency increased. At a minimum mass flow rate of 0.014 kg/s, a gap distance of 0.5 mm, slit width of 6 cm and a bed height of 7 cm, the maximum ΔT was achieved to be 27°C. The maximum efficiency of 82% was obtained for the bed height of 7 cm where the gap distance was minimum (0.5 mm) and the mass flux was the highest (0.057 kg/s) which shows significant improvement on the thermal efficiency in comparison to the conventional SAHs varied between 28% and 40% (Prasad et al., 2009). The results of the gap distances 0.5 mm and 1 mm showed that the SGSAH with 7 cm bed height performed better compared to the other two SGSAHs for higher mass flow rates (i.e., above 0.043 kg/s). For the gap distances 2 mm and 3 mm at lower mass flow rates (0.014-0.043) kg/s, the thermal performance of the SGSAH with 3 cm bed height was higher than the other two SGSAHs. The

efficiency of the SGSAH improved substantially after employing slit glazing compared to the conventional SAH.

6.2 The Effect of Width of the Glass Panes (Series II)

The results showed that the thermal efficiency increased with an increasing air mass flow rate. The maximum temperature rise was noted 28°C for a gap distance of 0.5 mm, slit width of 4 cm, and the lowest air mass flow rate of 0.014 kg/s. The maximum efficiency of 75% was obtained for a slit width of 4 cm, a lowest gap distance of 0.5 mm and maximum air mass flow rate of 0.029 kg/s. Summarizing, for each slit width, the best performance was achieved at the lowest gap distances and highest mass flow rates.

6.3 Comparison between SGSAH and UTC (Series III)

The results of both SGSAH and UTC are indicated that thermal efficiency increased by increasing the air mass flow rate. The maximum thermal efficiency of SGSAH and UTC was 54% and 44%, respectively; at highest mass flow rate (0.029 kg/s). The maximum temperature rise of SGSAH and UTC was 17℃ and 11℃, respectively; at the lowest mass flow rate (0.014 kg/s). Therefore by comparing the results, it is indicated that the thermal efficiency of SGSAH is 16% rather than a UTC.

REFERENCES

A. K. Bhargava, H. P. Garg, V. K. S. and R. B. M. (1985). Investigation on Double-Glazed Solar Air Heater Connected In Series with Rock Bed Solar Collector-Cum-Storage System. *Energy Convers. Mgmt*, *25*(2), 139–146.

Acir, A., Ata, I., & Canli, M. E. (2016). Investigation of effect of the circular ring turbulators on heat transfer augmentation and fluid flow characteristic of solar air heater. *Experimental Thermal and Fluid Science*, *77*, 45–54. https://doi.org/10.1016/j.expthermflusci.2016.04.012

Ahern, C., & Norton, B. (2015). Energy savings across EU domestic building stock by optimizing hydraulic distribution in domestic space heating systems. *Energy and Buildings*, *91*, 199–209. https://doi.org/10.1016/j.enbuild.2015.01.014

Akpinar, E. K., & Koçyiĝit, F. (2010). Energy and exergy analysis of a new flat-plate solar air heater having different obstacles on absorber plates. *Applied Energy*, *87*(11), 3438–3450. https://doi.org/10.1016/j.apenergy.2010.05.017

Akpinar, E. K., & Koçyiğit, F. (2010). Experimental investigation of thermal performance of solar air heater having different obstacles on absorber plates. *International Communications in Heat and Mass Transfer*, *37*(4), 416–421. https://doi.org/10.1016/j.icheatmasstransfer.2009.11.007

Al-kayiem, H. H., & Yassen, T. A. (2015). On the natural convection heat transfer in a rectangular passage solar air heater. *Solar Energy*, *112*, 310–318.

https://doi.org/10.1016/j.solener.2014.11.031

Alam, T., & Kim, M. H. (2016). Numerical study on thermal hydraulic performance improvement in solar air heater duct with semi ellipse shaped obstacles. *Energy*, *112*, 588–598. https://doi.org/10.1016/j.energy.2016.06.105

Al Mahdi, N., & Al Baharna, N. S. (1991). Thermal performance of an n-pass solar air heater. *Renewable Energy*, *I*(3), 527–532.

Aldabbagh, L. B. Y., Egelioglu, F., & Ilkan, M. (2010). Single and double pass solar air heaters with wire mesh as packing bed. *Energy*, *35*(9), 3783–3787. https://doi.org/10.1016/j.energy.2010.05.028

Alkilani, M. M., Sopian, K., Mat, S., & Alghoul, M. A. (2009). Output air temperature prediction in a solar air heater integrated with phase change material. *European Journal of Scientific Research*, *27*(3), 334–341.

Arulanandam, S. J., Hollands, K. G. T., & Brundrett, E. (1999). A CFD heat transfer analysis of the transpired solar collector under no-wind conditions. *Solar Energy*, *67*(1–3), 93–100. https://doi.org/10.1016/S0038-092X(00)00042-6

Badache, M., Rousse, D. R., Hallé, S., & Quesada, G. (2013). Experimental and numerical simulation of a two-dimensional unglazed transpired solar air collector. *Solar Energy*, *93*, 209–219. https://doi.org/10.1016/j.solener.2013.02.036

Badache M, Hallé S, R. D. (2012). A full 3^4 factorial experimental design for

efficiency optimization of an unglazed transpired solar collector prototype. *Solar Energy*, *86*(9), 2802–2810. https://doi.org/10.1016/j.solener.2012.06.020

Bahrehmand, D., Ameri, M., & Gholampour, M. (2015). Energy and exergy analysis of different solar air collector systems with forced convection. *Renewable Energy*, *83*, 1119–1130. https://doi.org/10.1016/j.renene.2015.03.009

Baritto, M., & Bracamonte, J. (2012). A dimensionless model for the outlet temperature of a nonisothermal flat plate solar collector for air heating. *Solar Energy*, *86*(1), 647–653. https://doi.org/10.1016/j.solener.2011.11.009

Bayrak, F., Oztop, H. F., & Hepbasli, A. (2013). Energy and exergy analyses of porous baffles inserted solar air heaters for building applications. *Energy and Buildings*, *57*, 338–345. https://doi.org/10.1016/j.enbuild.2012.10.055

Bekele, A., Mishra, M., & Dutta, S. (2014). Performance characteristics of solar air heater with surface mounted obstacles. *Energy Conversion and Management*, *85*, 603–611. https://doi.org/10.1016/j.enconman.2014.04.079

Bhagoria, J. L., Saini, J. S., & Solanki, S. C. (2002). Heat transfer coefficient and friction factor correlations for rectangular solar air heater duct having transverse wedge shaped rib roughness on the absorber plate. *Renewable Energy*, *25*(3), 341–369. https://doi.org/10.1016/S0960-1481(01)00057-X

Bhargava, A. K., Jha, R., & Gar, H. P. (1990). Analysis of a solar air heater with thermosyphon flow in one channel and forced flow in other channel. *Energy*

Convers. Mgmt, *30*(3), 231–234.

Bhushan, B., & Singh, R. (2012). Thermal and thermohydraulic performance of roughened solar air heater having protruded absorber plate. *Solar Energy*, *86*(11), 3388–3396. https://doi.org/10.1016/j.solener.2012.09.004

Bopche, S. B., & Tandale, M. S. (2009). Experimental investigations on heat transfer and frictional characteristics of a turbulator roughened solar air heater duct. *International Journal of Heat and Mass Transfer*, *52*(11–12), 2834–2848. https://doi.org/10.1016/j.ijheatmasstransfer.2008.09.039

Børvik, T., Hopperstad, O. S., Berstad, T., & Langseth, M. (2002). Perforation of 12 mm thick steel plates by 20 mm diameter projectiles with flat , hemispherical and conical noses Part II : numerical simulations. *International Journal of Impact Engineering*, *27*, 37–64. https://doi.org/10.1016/S0734-743X(01)00035-5

Bosseboeuf, D., Gynther, L., Lapillonne, B., & Pollier, K. (2015). *Energy Efficiency Trends and Policies in the Household and Tertiary Sectors An Analysis Based on the ODYSSEE and MURE Databases*.

Bouadila, S., Kooli, S., Lazaar, M., Skouri, S., & Farhat, A. (2013). Performance of a new solar air heater with packed-bed latent storage energy for nocturnal use. *Applied Energy*, *110*, 267–275. https://doi.org/10.1016/j.apenergy.2013.04.062

Caglayan, N., Alta, Z. D., & Ertekin, C. (2014). Experimental investigation of various type absorber plates for solar air heaters. *Journal of Agricultural*

Sciences, 1–12.

Chauhan, R., & Thakur, N. S. (2012). Heat transfer and friction characteristics of impinging jet solar air heater. *Journal of Renewable and Sustainable Energy*, *4*(4), 760–767. https://doi.org/10.1063/1.4747821

Chouksey, V. K., & Sharma, S. P. (2016). Investigations on thermal performance characteristics of wire screen packed bed solar air heater. *Solar Energy*, *132*, 591–605. https://doi.org/10.1016/j.solener.2016.03.040

Christensen, C, Hancock, E, Barker, G, Kutscher, C. (n.d.). Cost and performance predictions for advanced active solar concepts. In *Proceedings of The 1990 Annual Conference American Solar Energy Society, Inc* (pp. 275–280).

Christensen, Craig B, Charles F. Kutscher, M. Gawlik, B. (1997). Unglazed Transpired Solar Collector Having a Low Thermal Conductance Absorber. *Umted States Patent*.

Collins, M. R., & Abulkhair, H. (2014). An evaluation of heat transfer and effectiveness for unglazed transpired solar air heaters. *Solar Energy*, *99*, 231–245. https://doi.org/10.1016/j.solener.2013.11.012

Croitoru, C. V., Nastase, I., Bode, F. I., & Meslem, A. (2016). Thermodynamic investigation on an innovative unglazed transpired solar collector. *Solar Energy*, *131*, 21–29. https://doi.org/10.1016/j.solener.2016.02.029

Das, S. K., & Chakraverty, A. (1991). Performance of a solar collector with different glazing materials and their degradation under the condition prevailing in a solar collector. *Energy Convers. Mgmt*, *31*(3), 233–242. https://doi.org/10.1016/0196-8904(91)90077-V

Demirel, Y., & Kunc, S. (1987). Thermal performance study of a solar air heater with packed flow passage. *Energy Convers. Mgmt*, *27*(3), 317–325. https://doi.org/10.1104/pp.111.175976

Deo, N. S., Chander, S., & Saini, J. S. (2016). Performance analysis of solar air heater duct roughened with multigap V-down ribs combined with staggered ribs. *Renewable Energy*, *91*, 484–500. https://doi.org/10.1016/j.renene.2016.01.067

Dhiman, P., Thakur, N. S., & Chauhan, S. R. (2012). Thermal and thermohydraulic performance of counter and parallel flow packed bed solar air heaters. *Renewable Energy*, *46*, 259–268. https://doi.org/10.1016/j.renene.2012.03.032

Dhiman, P., Thakur, N. S., Kumar, A., & Singh, S. (2011). An analytical model to predict the thermal performance of a novel parallel flow packed bed solar air heater. *Applied Energy*, *88*(6), 2157–2167. https://doi.org/10.1016/j.apenergy.2010.12.033

Duffie, J. a., Beckman, W. a., & Worek, W. M. (2003). *Solar Engineering of Thermal Processes, 4nd ed. Journal of Solar Energy Engineering* (Vol. 116). https://doi.org/10.1115/1.2930068

Dymond, C., & Kutscher, C. (1997). Development of a flow distribution and design model for transpired solar collectors. *Solar Energy*, *60*(5), 291–300. https://doi.org/10.1016/S0038-092X(96)00157-0

E. C. Kern, J., & Russell, M. C. (1978). Combined photovoltaic and thermal hybrid collector systems. In *THE 13th IEEE PHOTOVOLTAIC*.

El-khawajah, M. F., Aldabbagh, L. B. Y., & Egelioglu, F. (2011). The effect of using transverse fins on a double pass flow solar air heater using wire mesh as an absorber. *Solar Energy*, *85*(7), 1479–1487. https://doi.org/10.1016/j.solener.2011.04.004

El-Sebaii, A. A., Aboul-Enein, S., Ramadan, M. R. I., Shalaby, S. M., & Moharram, B. M. (2011). Investigation of thermal performance of-double pass-flat and v-corrugated plate solar air heaters. *Energy*, *36*(2), 1076–1086. https://doi.org/10.1016/j.energy.2010.11.042

El-Sebaii, A. A., & Al-Snani, H. (2010). Effect of selective coating on thermal performance of flat plate solar air heaters. *Energy*, *35*(4), 1820–1828. https://doi.org/10.1016/j.energy.2009.12.037

Esen, H. (2008). Experimental energy and exergy analysis of a double-flow solar air heater having different obstacles on absorber plates. *Building and Environment*, *43*(6), 1046–1054. https://doi.org/10.1016/j.buildenv.2007.02.016

Esen, H., Ozgen, F., Esen, M., & Sengur, A. (2009a). Artificial neural network and

wavelet neural network approaches for modelling of a solar air heater. *Expert Systems with Applications*, *36*(8), 11240–11248. https://doi.org/10.1016/j.eswa.2009.02.073

Esen, H., Ozgen, F., Esen, M., & Sengur, A. (2009b). Modelling of a new solar air heater through least-squares support vector machines. *Expert Systems with Applications*, *36*(7), 10673–10682. https://doi.org/10.1016/j.eswa.2009.02.045

Fan, J., Yu, H., & Wei, Y. (2015). Residential energy-related carbon emissions in urban and rural China during 1996 – 2012 : From the perspective of five end-use activities. *Energy & Buildings*, *96*, 201–209. https://doi.org/10.1016/j.enbuild.2015.03.026

Fath, H. E. S. (1995). Thermal performance of a simple design solar air heater with built-in thermal energy storage system. *Energy Convers. Mgmt*, *36*(10), 989–997. https://doi.org/10.1016/0196-8904(94)00069-C

Fleck, B. A., Meier, R. M., & Matovic, M. D. (2002). A field study of the wind effects on the performance of an unglazed transpired solar collector. *Solar Energy*, *73*(3), 209–216. Retrieved from www.elsevier.com

Flores-Irigollen, A., Fernández, J. L., Rubio-Cerda, E., & Poujol, F. T. (2004). Heat transfer dynamics in an inflatable-tunnel solar air heater. *Renewable Energy*, *29*(8), 1367–1382. https://doi.org/10.1016/j.renene.2003.11.004

Gao, L., Bai, H., Fang, X., & Wang, T. (2013). Experimental study of a building-

integrated solar air heating system in cold climate of China. *Energy and Buildings*, *65*, 359–367. https://doi.org/10.1016/j.enbuild.2013.06.014

Gao, L., Bai, H., & Mao, S. (2014). Potential application of glazed transpired collectors to space heating in cold climates. *Energy Conversion and Management*, *77*, 690–699. https://doi.org/10.1016/j.enconman.2013.10.030

Gao, L., Bai, H., & Wu, X. (2013). Numerical analysis of heat transfer in unglazed transpired collectors based on field synergy principle. *Solar Energy*, *95*, 336–344. https://doi.org/10.1016/j.solener.2013.06.032

Gao, X., & Sundén, B. (2001). Heat transfer and pressure drop measurements in rib-roughened rectangular ducts. *Experimental Thermal and Fluid Science*, *24*(1–2), 25–34. https://doi.org/10.1016/S0894-1777(00)00054-6

Garg, H. P., Datta, G., & Bhargava, A. K. (1984). Some studies on the flow passage dimension for solar air heating collectors. *Energy Convers. Mgmt*, *24*(3), 181–184. https://doi.org/10.1016/0196-8904(84)90034-7

Gawande, V. B., Dhoble, A. S., & Zodpe, D. B. (2014). CFD analysis to study effect of circular vortex generator placed in inlet section to investigate heat transfer aspects of solar air heater. *TheScientificWorldJournal*, *2014*, 567257. https://doi.org/10.1155/2014/567257

Gawande, V. B., Dhoble, A. S., Zodpe, D. B., & Chamoli, S. (2016a). Analytical approach for evaluation of thermo hydraulic performance of roughened solar air

heater. *Case Studies in Thermal Engineering*, *8*, 19–31. https://doi.org/10.1016/j.csite.2016.03.003

Gawande, V. B., Dhoble, A. S., Zodpe, D. B., & Chamoli, S. (2016b). Experimental and CFD investigation of convection heat transfer in solar air heater with reverse L-shaped ribs. *Solar Energy*, *131*, 275–295. https://doi.org/10.1016/j.solener.2016.02.040

Gawlik, K., Christensen, C., & Kutscher, C. (2005). A Numerical and Experimental Investigation of Low-conductivity Unglazed, Transpired Solar Air Heaters. *Journal of Solar Energy Engineering*. https://doi.org/10.1115/1.1823494

Gill, R. S., Singh, S., & Singh, P. P. (2012). Low cost solar air heater. *Energy Conversion and Management*, *57*, 131–142. https://doi.org/10.1016/j.enconman.2011.12.019

Gunnewiek, L. H., Brundrett, E., & Hollands, K. G. T. (1996). Flow distribution in unglazed transpired plate solar air heaters of large area. *Solar Energy*, *58*(4–6), 227–237. https://doi.org/10.1016/S0038-092X(96)00083-7

Gunnewiek, L. H., Hollands, K. G. T., & Brundrett, E. (2002). Effect of wind on flow distribution in unglazed transpired. *Solar Energy*, *72*(4), 317–325. https://doi.org/10.1016/S0038-092X(02)00003-8

Gupta, M. K., & Kaushik, S. C. (2009). Performance evaluation of solar air heater for various artificial roughness geometries based on energy, effective and exergy

efficiencies. *Renewable Energy*, *34*(3), 465–476. https://doi.org/10.1016/j.renene.2008.06.001

H.P, Garg, V.K, Sharma, R.B, Mahajan, And, Bhargave, A. K. (1985). Experimental study of an inexpensive solar collector cum storage system for agricultural uses. *Solar Energy*, *35*(4), 321–331.

Handoyo, E. A., Ichsani, D., Prabowo, & Sutardi. (2016). Numerical studies on the effect of delta-shaped obstacles' spacing on the heat transfer and pressure drop in v-corrugated channel of solar air heater. *Solar Energy*, *131*, 47–60. https://doi.org/10.1016/j.solener.2016.02.031

Hanemann, M., Labeaga, J. M., & López-otero, X. (2013). *Energy Demand for Heating : Short Run and Long Run Energy Demand for Heating : Short Run and Long Run*.

Hans, V. S., Saini, R. P., & Saini, J. S. (2010). Heat transfer and friction factor correlations for a solar air heater duct roughened artificially with multiple v-ribs. *Solar Energy*, *84*(6), 898–911. https://doi.org/10.1016/j.solener.2010.02.004

Hilliaho, K., Köliö, A., Pakkala, T., Lahdensivu, J., & Vinha, J. (2016). Effects of added glazing on Balcony indoor temperatures: Field measurements. *Energy and Buildings*, *128*, 458–472. https://doi.org/10.1016/j.enbuild.2016.07.025

Ho, C.-D., Lin, C.-S., Yang, T.-J., & Chao, C.-C. (2014). Recycle Effect on Device Performance of Wire Mesh Packed Double-Pass Solar Air Heaters. *Energies*,

7(11), 7568–7585. https://doi.org/10.3390/en7117568

Ho, C. D., Chang, H., Lin, C. S., Chao, C. C., & Tien, Y. E. (2016). Device performance improvement of double-pass wire mesh packed solar air heaters under recycling operation conditions. *Energies*, *9*(2), 1–10. https://doi.org/10.3390/en9020068

Ho, C. D., Chang, H., Wang, R. C., & Lin, C. S. (2012). Performance improvement of a double-pass solar air heater with fins and baffles under recycling operation. *Applied Energy*, *100*, 155–163. https://doi.org/10.1016/j.apenergy.2012.03.065

Ho, C. D., Yeh, H. M., & Chen, T. C. (2011). Collector efficiency of upward-type double-pass solar air heaters with fins attached. *International Communications in Heat and Mass Transfer*, *38*(1), 49–56. https://doi.org/10.1016/j.icheatmasstransfer.2010.09.015

Ho, C. D., Yeh, H. M., Cheng, T. W., Chen, T. C., & Wang, R. C. (2009). The influences of recycle on performance of baffled double-pass flat-plate solar air heaters with internal fins attached. *Applied Energy*, *86*(9), 1470–1478. https://doi.org/10.1016/j.apenergy.2008.12.013

Hollick, J. C. (1998). Solar cogeneration panels. *Renewable Energy*, *15*(1–4 pt 1), 195–200. https://doi.org/10.1016/S0960-1481(98)00154-2

Hollick, J. C. (1999). Commercial scale solar drying. *Renewable Energy*, *16*, 714–719. https://doi.org/10.1016/S0960-1481(98)00258-4

Holman, J. P. (1989). *Experimental methods for engineers*. McGraw-Hill, 453 New York.

Hu, J., Sun, X., Xu, J., & Li, Z. (2013). Numerical analysis of mechanical ventilation solar air collector with internal baffles. *Energy and Buildings*, *62*, 230–238. https://doi.org/10.1016/j.enbuild.2013.03.015

Indrajit, Bansal, N. K., & Garg, H. P. (1985). An experimental study on a finned type and non-porous type solar air heater with a solar simulator. *Energy Convers. Mgmt*, *25*(2), 135–138.

International Energy Agency. (2012). *Energy Technology Perspectives 2012*. *Energy Technology Perspectives 2012*. OECD Publishing. https://doi.org/10.1787/energy_tech-2012-en

Jaurker, A. R., Saini, J. S., & Gandhi, B. K. (2006). Heat transfer and friction characteristics of rectangular solar air heater duct using rib-grooved artificial roughness. *Solar Energy*, *80*(8), 895–907. https://doi.org/10.1016/j.solener.2005.08.006

Jin, D., Zhang, M., Wang, P., & Xu, S. (2015). Numerical investigation of heat transfer and fluid flow in a solar air heater duct with multi V-shaped ribs on the absorber plate. *Energy*, *89*, 178–190. https://doi.org/10.1016/j.energy.2015.07.069

Joshi, A. S., & Tiwari, A. (2007). Energy and exergy efficiencies of a hybrid

photovoltaic–thermal (PV/T) air collector. *Renewable Energy*, *32*(13), 2223–2241. https://doi.org/10.1016/j.renene.2006.11.013

Karmare, S. V., & Tikekar, A. N. (2009). Experimental investigation of optimum thermohydraulic performance of solar air heaters with metal rib grits roughness. *Solar Energy*, *83*(1), 6–13. https://doi.org/10.1016/j.solener.2008.05.017

Karmare, S. V., & Tikekar, A. N. (2010). Analysis of fluid flow and heat transfer in a rib grit roughened surface solar air heater using CFD. *Solar Energy*, *84*(3), 409–417. https://doi.org/10.1016/j.solener.2009.12.011

Karwa, R. (2003). Experimental studies of augmented heat transfer and friction in asymmetrically heated rectabgular ducts with ribs on the heated wall in transverse, inclined, v-continous and v-discrete pattern. *International Communications in Heat and Mass Transfer*, *30*(2), 241–250. https://doi.org/10.1016/S0735-1933(03)00035-6

Karwa, R., & Chauhan, K. (2010). Performance evaluation of solar air heaters having v-down discrete rib roughness on the absorber plate. *Energy*, *35*(1), 398–409. https://doi.org/10.1016/j.energy.2009.10.007

Kasperski, J., & Nemś, M. (2013). Investigation of thermo-hydraulic performance of concentrated solar air-heater with internal multiple-fin array. *Applied Thermal Engineering*, *58*(1–2), 411–419. https://doi.org/10.1016/j.applthermaleng.2013.04.018

Kumar, A., Bhagoria, J. L., & Sarviya, R. M. (2009). Heat transfer and friction correlations for artificially roughened solar air heater duct with discrete W-shaped ribs. *Energy Conversion and Management*, *50*(8), 2106–2117. https://doi.org/10.1016/j.enconman.2009.01.025

Kumar, A., Saini, R. P., & Saini, J. S. (2012). Experimental investigation on heat transfer and fluid flow characteristics of air flow in a rectangular duct with Multi v-shaped rib with gap roughness on the heated plate. *Solar Energy*, *86*(6), 1733–1749. https://doi.org/10.1016/j.solener.2012.03.014

Kumar, S., & Saini, R. P. (2009). CFD based performance analysis of a solar air heater duct provided with artificial roughness. *Renewable Energy*, *34*(5), 1285–1291. https://doi.org/10.1016/j.renene.2008.09.015

Kutscher, C. F. (1992). *An investigation of heat transfer for air flow through low porostiy plates*. University of Colorado, Department of Mechanical Engineering; Ph.D. Thesis.

Kutscher, C. F., Christensen, C. B., & Barker, G. M. (1993). Unglazed Transpired Solar Collectors: Heat Loss Theory. *Journal of Solar Energy Engineering*, *115*(3), 182. https://doi.org/10.1115/1.2930047

Lanjewar, A., Bhagoria, J. L., & Sarviya, R. M. (2011). Experimental study of augmented heat transfer and friction in solar air heater with different orientations of W-Rib roughness. *Experimental Thermal and Fluid Science*, *35*(6), 986–995. https://doi.org/10.1016/j.expthermflusci.2011.01.019

Lanjewar, A., Bhagoria, J. L., & Sarviya, R. M. (2011). Heat transfer and friction in solar air heater duct with W-shaped rib roughness on absorber plate. *Energy*, *36*(7), 4531–4541. https://doi.org/10.1016/j.energy.2011.03.054

Layek, A., Saini, J. S., & Solanki, S. C. (2007). Second law optimization of a solar air heater having chamfered rib-groove roughness on absorber plate. *Renewable Energy*, *32*(12), 1967–1980. https://doi.org/10.1016/j.renene.2006.11.005

Layek, A., Saini, J. S., & Solanki, S. C. (2009). Effect of chamfering on heat transfer and friction characteristics of solar air heater having absorber plate roughened with compound turbulators. *Renewable Energy*, *34*(5), 1292–1298. https://doi.org/10.1016/j.renene.2008.09.016

Leon, M. A., & Kumar, S. (2007). Mathematical modeling and thermal performance analysis of unglazed transpired solar collectors. *Solar Energy*, *81*(1), 62–75. https://doi.org/10.1016/j.solener.2006.06.017

Li, X., Li, C., & Li, B. (2016). Net heat gain assessment on a glazed transpired solar air collector with slit-like perforations. *Applied Thermal Engineering*, *99*, 1–10. https://doi.org/10.1016/j.applthermaleng.2015.12.069

Mahmood, A. J., Aldabbagh, L. B. Y., & Egelioglu, F. (2015). Investigation of single and double pass solar air heater with transverse fins and a package wire mesh layer. *Energy Conversion and Management*, *89*, 599–607. https://doi.org/10.1016/j.enconman.2014.10.028

Mittal, M. K., & Varshney, L. (2006). Optimal thermohydraulic performance of a wire mesh packed solar air heater. *Solar Energy*, *80*(9), 1112–1120. https://doi.org/10.1016/j.solener.2005.10.004

Mittal, M. K., Varun, Saini, R. P., & Singal, S. K. (2007). Effective efficiency of solar air heaters having different types of roughness elements on the absorber plate. *Energy*, *32*(5), 739–745. https://doi.org/10.1016/j.energy.2006.05.009

Mohamad, a. a. (1997). High efficiency solar air heater. *Solar Energy*, *60*(2), 71–76. https://doi.org/10.1016/S0038-092X(96)00163-6

Momin, A.-M. E., Saini, J. S., & Solanki, S. C. (2001). Heat transfer and friction in solar air heater duct with V-shaped rib roughness on absorber plate. *International Journal of Heat and Mass Transfer*, *45*, 3383–3396. https://doi.org/10.1016/j.energy.2011.03.054

Nemś, M., & Kasperski, J. (2016). Experimental investigation of concentrated solar air-heater with internal multiple-fin array. *Renewable Energy*, *97*, 722–730. https://doi.org/10.1016/j.renene.2016.06.038

Njomo, D. (1991). Modelling the heat exchanges in a solar air heater with a cover partially transparent to infrared radiation. *Energy Convers. Mgmt*, *31*(5), 495–503.

Nowzari, R., Aldabbagh, L. B. Y., & Egelioglu, F. (2014). Single and double pass solar air heaters with partially perforated cover and packed mesh. *Energy*, *73*,

694–702. https://doi.org/10.1016/j.energy.2014.06.069

Omojaro, A. P., & Aldabbagh, L. B. Y. (2010). Experimental performance of single and double pass solar air heater with fins and steel wire mesh as absorber. *Applied Energy*, *87*(12), 3759–3765. https://doi.org/10.1016/j.apenergy.2010.06.020

Pandey, N. K., Bajpai, V. K., & Varun. (2016). Experimental investigation of heat transfer augmentation using multiple arcs with gap on absorber plate of solar air heater. *Solar Energy*, *134*, 314–326. https://doi.org/10.1016/j.solener.2016.05.007

Paya-Marin, M. A., Lim, J. B. P., Chen, J. F., Lawson, R. M., & Gupta, B. Sen. (2015). Large scale test of a novel back-pass non-perforated unglazed solar air collector. *Renewable Energy*, *83*, 871–880. https://doi.org/10.1016/j.renene.2015.05.039

Prasad, S. B., Saini, J. S., & Singh, K. M. (2009). Investigation of heat transfer and friction characteristics of packed bed solar air heater using wire mesh as packing material. *Solar Energy*, *83*(5), 773–783. https://doi.org/10.1016/j.solener.2008.11.011

Priyam, A., & Chand, P. (2016). Thermal and thermohydraulic performance of wavy finned absorber solar air heater. *Solar Energy*, *130*, 250–259. https://doi.org/10.1016/j.solener.2016.02.030

Promvonge, P., Khanoknaiyakarn, C., Kwankaomeng, S., & Thianpong, C. (2011). Thermal behavior in solar air heater channel fitted with combined rib and delta-winglet. *International Communications in Heat and Mass Transfer*, *38*(6), 749–756. https://doi.org/10.1016/j.icheatmasstransfer.2011.03.014

Rad, H. M., & Ameri, M. (2016). Energy and exergy study of unglazed transpired collector-2stage. *Solar Energy*, *132*, 570–586. https://doi.org/10.1016/j.solener.2016.03.045

Rajaseenivasan, T., Srinivasan, S., & Srithar, K. (2015). Comprehensive study on solar air heater with circular and V-type turbulators attached on absorber plate. *Energy*, *88*, 863–873. https://doi.org/10.1016/j.energy.2015.07.020

Sabzpooshani, M., Mohammadi, K., & Khorasanizadeh, H. (2014). Exergetic performance evaluation of a single pass baffled solar air heater. *Energy*, *64*, 697–706. https://doi.org/10.1016/j.energy.2013.11.046

Sahu, M. M., & Bhagoria, J. L. (2005). Augmentation of heat transfer coefficient by using 90? broken transverse ribs on absorber plate of solar air heater. *Renewable Energy*, *30*(13), 2057–2073. https://doi.org/10.1016/j.renene.2004.10.016

Saini, R. P., & Verma, J. (2008). Heat transfer and friction factor correlations for a duct having dimple-shape artificial roughness for solar air heaters. *Energy*, *33*(8), 1277–1287. https://doi.org/10.1016/j.energy.2008.02.017

Satcunanathan, S., & Deonarine, S. (1973). A two-pass solar air heater. *Solar*

Energy, *15*(1), 41–49. https://doi.org/10.1016/0038-092X(73)90004-2

Saxena, A., Agarwal, N., & Srivastava, G. (2013). Design and performance of a solar air heater with long term heat storage. *International Journal of Heat and Mass Transfer*, *60*(1), 8–16. https://doi.org/10.1016/j.ijheatmasstransfer.2012.12.044

Sethi, M., Varun, & Thakur, N. S. (2012). Correlations for solar air heater duct with dimpled shape roughness elements on absorber plate. *Solar Energy*, *86*(9), 2852–2861. https://doi.org/10.1016/j.solener.2012.06.024

Sharma, V. K., Rizzi, G., & Garg, H. P. (1991). Design and development of a matrix type solar air heater. *Energy Conversion and Management*, *31*(4), 379–388. https://doi.org/10.1016/0196-8904(91)90018-E

Sims, R. E. H. (2003). *Bioenergy to mitigate for climate change and meet the needs of society, the economy and the environment*. *Mitigation and Adaptation Strategies for Global Change* (Vol. 8). https://doi.org/10.1023/B:MITI.0000005614.51405.ce

Singh, A., & Bhagoria, J. L. (2014). A numerical investigation of square sectioned transverse rib roughened solar air heater. *International Journal of Thermal Sciences*, *79*, 111–131. https://doi.org/10.1016/j.ijthermalsci.2014.01.008

Singh, S., Chander, S., & Saini, J. S. (2011). Heat transfer and friction factor correlations of solar air heater ducts artificially roughened with discrete V-down ribs. *Energy*, *36*(8), 5053–5064. https://doi.org/10.1016/j.energy.2011.05.052

Singh, S., Chander, S., & Saini, J. S. (2012a). Exergy based analysis of solar air heater having discrete V-down rib roughness on absorber plate. *Energy*, *37*(1), 749–758. https://doi.org/10.1016/j.energy.2011.09.040

Singh, S., Chander, S., & Saini, J. S. (2012b). Investigations on thermo-hydraulic performance due to flow-attack-angle in V-down rib with gap in a rectangular duct of solar air heater. *Applied Energy*, *97*, 907–912. https://doi.org/10.1016/j.apenergy.2011.11.090

Singh, S., Chander, S., & Saini, J. S. (2015). Thermo-hydraulic performance due to relative roughness pitch in V-down rib with gap in solar air heater duct - Comparison with similar rib roughness geometries. *Renewable and Sustainable Energy Reviews*, *43*, 1159–1166. https://doi.org/10.1016/j.rser.2014.11.087

Singh, S., Singh, B., Hans, V. S., & Gill, R. S. (2015). CFD (computational fluid dynamics) investigation on Nusselt number and friction factor of solar air heater duct roughened with non-uniform cross-section transverse rib. *Energy*, *84*, 509–517. https://doi.org/10.1016/j.energy.2015.03.015

Skullong, S., Kwankaomeng, S., Thianpong, C., & Promvonge, P. (2014). Thermal performance of turbulent flow in a solar air heater channel with rib-groove turbulators. *International Communications in Heat and Mass Transfer*, *50*, 34–43. https://doi.org/10.1016/j.icheatmasstransfer.2013.11.001

Skullong, S., Promvonge, P., Thianpong, C., & Pimsarn, M. (2016). Thermal performance in solar air heater channel with combined wavy-groove and

perforated-delta wing vortex generators. *Applied Thermal Engineering*, *100*, 611–620. https://doi.org/10.1016/j.applthermaleng.2016.01.107

Solanki, S. C., Dubey, S., & Tiwari, A. (2009). Indoor simulation and testing of photovoltaic thermal (PV/T) air collectors. *Applied Energy*, *86*(11), 2421–2428. https://doi.org/10.1016/j.apenergy.2009.03.013

Sriromreun, P., Thianpong, C., & Promvonge, P. (2012). Experimental and numerical study on heat transfer enhancement in a channel with Z-shaped baffles. *International Communications in Heat and Mass Transfer*, *39*(7), 945–952. https://doi.org/10.1016/j.icheatmasstransfer.2012.05.016

Sugantharaj, G., Vijay, K., & Kulundaivel, K. (2016). Performances of packed bed double pass solar air heater with different inclinations and transverse wire mesh with different intervals. *Thermal Science*, *20*(1), 175–183. https://doi.org/10.2298/TSCI131015085S

Summers DN, Mitchell JW, Klein SA, B. W. (1996). Thermal simulation and economic assessment of unglazed transipred collector systems. *Wisconsin Energy Bureau, University of Wisconsin, USA*.

Sun, W., Ji, J., & He, W. (2010). Influence of channel depth on the performance of solar air heaters. *Energy*, *35*(10), 4201–4207. https://doi.org/10.1016/j.energy.2010.07.006

Tamna, S., Skullong, S., Thianpong, C., & Promvonge, P. (2014). Heat transfer

behaviors in a solar air heater channel with multiple V-baffle vortex generators. *Solar Energy*, *110*, 720–735. https://doi.org/10.1016/j.solener.2014.10.020

Tanda, G. (2011). Performance of solar air heater ducts with different types of ribs on the absorber plate. *Energy*, *36*(11), 6651–6660. https://doi.org/10.1016/j.energy.2011.08.043

Thirugnanasambandam, M., Iniyan, S., & Goic, R. (2010). A review of solar thermal technologies. *Renewable and Sustainable Energy Reviews*, *14*(1), 312–322. https://doi.org/10.1016/j.rser.2009.07.014

Toğrul, I. T., & Pehlivan, D. (2005). Effect of packing in the airflow passage on the performance of a solar air-heater with conical concentrator. *Applied Thermal Engineering*, *25*(8–9), 1349–1363. https://doi.org/10.1016/j.applthermaleng.2004.08.015

Türk Toğrul, İ., & Pehlıvan, D. (2003). The performance of a solar air heater with conical concentrator under forced convection. *International Journal of Thermal Sciences*, *42*(6), 571–581. https://doi.org/10.1016/S1290-0729(03)00023-1

UNDP. (2000). World Energy Assessment. Energy and the challenge of Sustainability. In *UNDP* (p. 506). New York. Retrieved from 92-1-126126-0

Ürge-Vorsatz, D., Cabeza, L. F., Serrano, S., Barreneche, C., & Petrichenko, K. (2015). Heating and cooling energy trends and drivers in buildings. *Renewable and Sustainable Energy Reviews*, *41*, 85–98.

https://doi.org/10.1016/j.rser.2014.08.039

Van Decker, G. W. E., Hollands, K. G. T., & Brunger, A. P. (2001). Heat-exchange relations for unglazed transpired solar collectors with circular holes on a square or triangular pitch. *Solar Energy*, *71*(1), 33–46. https://doi.org/10.1016/S0038-092X(01)00014-7

Varun, Patnaik, A., Saini, R. P., Singal, S. K., & Siddhartha. (2009). Performance prediction of solar air heater having roughened duct provided with transverse and inclined ribs as artificial roughness. *Renewable Energy*, *34*(12), 2914–2922. https://doi.org/10.1016/j.renene.2009.04.030

Varun, Saini, R. P., & Singal, S. K. (2007). A review on roughness geometry used in solar air heaters. *Solar Energy*, *81*(11), 1340–1350. https://doi.org/10.1016/j.solener.2007.01.017

Varun, & Siddhartha. (2010). Thermal performance optimization of a flat plate solar air heater using genetic algorithm. *Applied Energy*, *87*(5), 1793–1799. https://doi.org/10.1016/j.apenergy.2009.10.015

Vasan, N., & Stathopoulos, T. (2014). Experimental study of wind effects on unglazed transpired collectors. *Solar Energy*, *101*, 138–149. https://doi.org/10.1016/j.solener.2013.11.037

Vaziri, R., Ilkan, M., & Egelioglu, F. (2015). Experimental performance of perforated glazed solar air heaters and unglazed transpired solar air heater. *Solar*

Energy, *119*, 251–260. https://doi.org/10.1016/j.solener.2015.06.043

Wazed, M. A., Nukman, Y., & Islam, M. T. (2010). Design and fabrication of a cost effective solar air heater for Bangladesh. *Applied Energy*, *87*(10), 3030–3036. https://doi.org/10.1016/j.apenergy.2010.02.014

Wijeysundera, N. E., Ah, L. L., & Tjioe, L. E. (1982). Thermal performance study of two-pass solar air heaters. *Solar Energy*, *28*(5), 363–370. https://doi.org/10.1016/0038-092X(82)90253-5

Yadav, A. S., & Bhagoria, J. L. (2013). A CFD (computational fluid dynamics) based heat transfer and fluid flow analysis of a solar air heater provided with circular transverse wire rib roughness on the absorber plate. *Energy*, *55*, 1127–1142. https://doi.org/10.1016/j.energy.2013.03.066

Yadav, A. S., & Bhagoria, J. L. (2014). A CFD based thermo-hydraulic performance analysis of an artificially roughened solar air heater having equilateral triangular sectioned rib roughness on the absorber plate. *International Journal of Heat and Mass Transfer*, *70*, 1016–1039. https://doi.org/10.1016/j.ijheatmasstransfer.2013.11.074

Yadav, S., Kaushal, M., Varun, & Siddhartha. (2013). Nusselt number and friction factor correlations for solar air heater duct having protrusions as roughness elements on absorber plate. *Experimental Thermal and Fluid Science*, *44*(5), 34–41. https://doi.org/10.1016/j.expthermflusci.2012.05.011

Yadav, S., Kaushal, M., Varun, & Siddhartha. (2014). Exergetic performance evaluation of solar air heater having arc shape oriented protrusions as roughness element. *Solar Energy*, *105*, 181–189. https://doi.org/10.1016/j.solener.2014.04.001

Yang, M., Yang, X., Li, X., Wang, Z., & Wang, P. (2014). Design and optimization of a solar air heater with offset strip fin absorber plate. *Applied Energy*, *113*, 1349–1362. https://doi.org/10.1016/j.apenergy.2013.08.091

Yeh, H.-M., & Ho, C.-D. (2009). Solar air heaters with external recycle. *Applied Thermal Engineering*, *29*(8–9), 1694–1701. https://doi.org/10.1016/j.applthermaleng.2008.07.027

Yeh, H. M., Ho, C. D., & Hou, J. Z. (1999). The improvement of collector efficiency in solar air heaters by simultaneously air flow over and under the absorbing plate. *Energy*, *24*(10), 857–871. https://doi.org/10.1016/S0360-5442(99)00043-2

Zheng, W., Li, B., Zhang, H., You, S., Li, Y., & Ye, T. (2016). Thermal characteristics of a glazed transpired solar collector with perforating corrugated plate in cold regions, *109*. https://doi.org/10.1016/j.energy.2016.05.064